Foundations of Computational Mathematics manuscript No.
(will be inserted by the editor)

Exact non-reflecting boundary conditions revisited: well-posedness and stability

Sofia Eriksson · **Jan Nordström**

Received: date / Accepted: date

Abstract Exact non-reflecting boundary conditions for a linear incompletely parabolic system in one dimension have been studied. The system is a model for the linearized compressible Navier-Stokes equations, but is less complicated which allows for a detailed analysis without approximations. It is shown that well-posedness is a fundamental property of the exact non-reflecting boundary conditions. By using summation by parts operators for the numerical approximation and a weak boundary implementation, it is also shown that energy stability follows automatically.

Keywords Non-reflecting boundary conditions · Well-posedness · Summation by parts · Weak boundary implementation · Stability

Mathematics Subject Classification (2010) 65M12 · 65M06 · 35M33

1 Introduction

In computational physics one often encounters the problem of how to limit the computational domain and introduce artificial boundary conditions (ABC). Such boundaries will generate non-physical disturbances, and in many applications, especially where high accuracy is required, it is essential that these disturbances are minimized. If the errors produced at the boundary stay localized, the boundary conditions have limited influence on the solution and a simple boundary condition of Dirichlet type

S. Eriksson
Department of Mathematics, Technische Universität Darmstadt, 64293 Darmstadt, Germany
Tel.: +49-6151-16-2085
Fax: +49-6151-16-2747
E-mail: eriksson@mathematik.tu-darmstadt.de

J. Nordström
Department of Mathematics, Linköping University, 58183 Linköping, Sweden
Tel.: +46-13-281459
Fax: +46-13-100746
E-mail: jan.nordstrom@liu.se

can be used. However, this scenario is rare and often a significant portion of the errors will reflect back.

In the classical paper [9], exact boundary closures are constructed in transformed space for the wave equation. The approach is to express the solution as a superposition of waves, and eliminate the incoming waves at the boundaries. Similar techniques for deriving the non-reflecting boundary conditions (NRBC), for other types of equations, are used in [20,14,24]. Note that these conditions are exact, but formulated in transformed space.

The area of ABC's has been the subject of massive research, especially for hyperbolic problems, [12,15,13,21,5]. In [22,19,18,24], approximative NRBC's for different problems of advection-diffusion type are considered. For an extensive review on ABC's, see [47]. An alternative to the above mentioned methods is to introduce zones outside the artificial boundary, where the governing equations are modified such that waves are damped. When these zones are constructed to be exactly non-reflecting, they are called perfectly matched layers (PML), see [6,25,4,3,32,28]. Yet another strategy is to construct exact NRBC's for the discrete problem directly, as is done in [49,48,27,23,40]

Exact NRBC's are in most cases global in space and time, and can therefore be cumbersome to implement numerically. For special geometries it is possible to localize the boundary conditions in time while still keeping them exact. See [20] for details on exact and approximate NRBC on special computational domains. These techniques are unfortunately not always feasible, and in [35] computations are performed for the Schrödinger equation with the exact NRBC's transformed back to time-domain using convolution quadratures. See [2] for other approximations of time convolution.

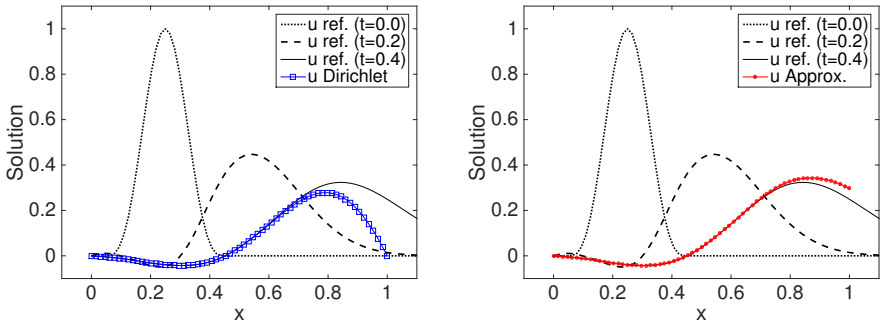

(a) Solution at $t = 0.4$ (b) Solution at $t = 0.4$

Fig. 1.1 The solution to equation (2.1), with initial condition given by (8.1). At $x = 1$ either (a) a Dirichlet boundary condition, or (b) a zeroth order approximate NRBC, is imposed.

Due to the difficulties associated with the transformed domains, it is common to approximate or localize the NRBC's in space or time. In [9], where the exact NRBC's are made local in space and time using expansions, it is shown that some approxima-

tions are well-posed, and some ill-posed. To achieve boundary conditions that give sufficiently small reflections, high order expansions are necessary, which typically yields an ill-posed problem. For low order expansions it is easier to obtain well-posedness, and the results are clearly better than the results obtained using Dirichlet boundary conditions, see Figure 1.1.

The main drawback with the approximative NRBC's is that they ruin the increased accuracy expected from mesh refinement of the interior scheme. From Table 1.1 it is evident that the solution obtained using the low order NRBC's, although it looks promising in Figure 1.1(b), does not converge to the correct solution as we refine the mesh. There will always be an order one error remaining in the solution, because the lowest order NRBC's (since they are not exact) describes and converges to another solution than the infinite domain solution.

Table 1.1 Results obtained using the approximative, low order NRBC.

N	Error(u)	ratio	conv. rate
16	0.01390245		
32	0.01407590	0.9877	-0.0179
64	0.01409017	0.9990	-0.0015
128	0.01409115	0.9999	-0.0001

In this paper we follow the work and technique in [9] to some extent, but with a slightly different purpose. Our goal is to show that the exact NRBC's result in a well-posed problem, and that this leads to energy estimates both for the continuous and the discrete formulation of the problem. We can thus, by a chain of arguments, guarantee a stable numerical procedure. We will also extend the results in [9] by considering an incompletely parabolic system which we see as a model of the compressible Navier-Stokes equations in the linear regime. Our model problem lends itself to a more detailed analysis, and yet keeps the characteristics of the full problem. Most importantly; the continuous boundary conditions will not be approximated.

The exact NRBC's are derived in Laplace transformed space, and are hence global in time. They are thereafter transformed back for the numerical simulations. We use high order accurate finite difference techniques, see [36, 7, 44, 38], such that the error originating from the interior discretization is kept at a minimum. The stability in combination with our finite difference method results in a reliable, efficient and high order accurate method.

The studied system is in one space dimension. To generalize the technique in this paper to the multidimensional case, it must be possible to handle the dimensions tangential to the boundary using appropriate expansions, for example Fourier transforms or spherical harmonics. This in turn require special computational domains, for example cylindrical or spherical domains.

As mentioned earlier, high order expansions of NRBC's are often found to be ill-posed, but given that the exact NRBC's yields a well-posed problem it is likely that well-posed high order approximations exist, which motivates increased efforts to find the right way to approximate the exact NRBC's.

The rest of the paper is organized as follows. In Sect. 2 we formulate the continuous problem. In Sect. 3 exact non-reflecting boundary conditions are derived. In Sect. 4 we show that the continuous problem is well-posed when using the non-reflecting boundary conditions, and that this leads to an energy estimate. The corresponding semi-discrete problem is presented in Sect. 5. In Sect. 6, a boundary procedure that leads to energy stability is presented. Then, in Sect. 7, numerical details on how the boundary procedure in Laplace space is transformed to time domain are given. In Sect. 8 numerical experiments are presented and conclusions are drawn in Sect. 9.

2 The continuous problem formulation

Consider the linear 2×2 system of partial differential equations

$$\begin{aligned} U_t + AU_x - BU_{xx} &= F, & x \in [x_L, x_R], \quad t \geq 0 \\ U &= f, & x \in [x_L, x_R], \quad t = 0 \\ L_{L,R}U &= g_{L,R}, & x = x_{L,R}, \quad t \geq 0, \end{aligned} \tag{2.1}$$

where

$$U = \begin{bmatrix} p \\ u \end{bmatrix}, \qquad A = \begin{bmatrix} v & c \\ c & v \end{bmatrix}, \qquad B = \begin{bmatrix} 0 & 0 \\ 0 & \varepsilon \end{bmatrix}, \qquad v > 0.$$

$F(x,t)$ is the forcing function and $f(x)$ is the initial data. The operators $L_L(t)$ and $L_R(t)$ and the data $g_L(t)$ and $g_R(t)$ in the boundary conditions $L_{L,R}U = g_{L,R}$ are at this stage unknown, and the aim is to derive them such that the solution $U(x,t)$ will resemble the solution obtained if we would have $x \in (-\infty, +\infty)$. The data in F, f, $L_{L,R}$ and $g_{L,R}$ is assumed to be sufficiently smooth and compatible with the problem, see also Remark 3.2. The Initial Boundary Value Problem (IBVP) (2.1) is incompletely parabolic and hence it has most of the properties and difficulties associated with the linearized compressible Navier-Stokes equations. Throughout the paper we assume $v > 0$. Exactly the same analysis can be done for negative values of v.

The Laplace transformed version of (2.1) is

$$\begin{aligned} s\hat{U} + A\hat{U}_x - B\hat{U}_{xx} &= \hat{F} + f, & x \in [x_L, x_R] \\ \hat{L}_{L,R}\hat{U} &= \hat{g}_{L,R}, & x = x_{L,R}, \end{aligned} \tag{2.2}$$

where $s = \eta + \xi i$ is the dual variable to time, and $\hat{U} = [\ \hat{p},\ \hat{u}\ ]^T$ is defined as

$$\hat{U}(x,s) = \mathscr{L}\{U(x,t)\} = \int_0^\infty e^{-st} U(x,t)\, dt, \qquad \mathscr{L}\{U'(x,t)\} = s\hat{U}(x,s) - U(x,0).$$

For the Laplace transform to be valid η must be large enough such that the integrand exists. Further, for later purposes we assume that $U(\cdot,t) \in L^2[x_L, x_R]$.To simplify the analysis, we write (2.2) on first order form by introducing $\hat{w} = \hat{u}_x$, which yields

$$\begin{aligned} \bar{S}\bar{U} + \bar{A}\bar{U}_x &= \bar{F}, & x \in [x_L, x_R] \\ \bar{L}_{L,R}\bar{U} &= \hat{g}_{L,R}, & x = x_{L,R}, \end{aligned} \tag{2.3}$$

where $\bar{S} = diag(s,s,1)$ and where

$$\bar{A} = \begin{bmatrix} v & c & 0 \\ c & v & -\varepsilon \\ 0 & -1 & 0 \end{bmatrix}, \qquad \bar{U} = \begin{bmatrix} \hat{p} \\ \hat{u} \\ \hat{w} \end{bmatrix}, \qquad \bar{F} = \begin{bmatrix} \hat{F}_1 + f_1 \\ \hat{F}_2 + f_2 \\ 0 \end{bmatrix}.$$

The solution to (2.3) consists of a homogenous and a particular part, such that $\bar{U} = \bar{U}_h + \bar{U}_p$. The particular solution $\bar{U}_p$ (which depends on the data $\bar{F}$) is assumed to be known. The ansatz $\bar{U}_h = e^{\kappa x}\Psi$ leads to a generalized eigenvalue problem for $\kappa(s)$ and $\Psi(s)$ on the form $(\bar{S} + \kappa\bar{A})\Psi = 0$. This eigenvalue problem can only have non-trivial solutions $\Psi \neq 0$ if the determinant $|\bar{S} + \kappa\bar{A}|$ is zero. Written out explicitly the determinant is

$$|\bar{S} + \kappa\bar{A}| = q(\kappa,s), \qquad q(\kappa,s) = s^2 + 2sv\kappa + (v^2 - c^2 - s\varepsilon)\kappa^2 - \varepsilon v\kappa^3. \tag{2.4}$$

Solving $q(\kappa,s) = 0$ for the eigenvalues κ, and assuming that the three roots κ_j are distinct, gives the general homogeneous solution

$$\bar{U}_h = \sum_{j=1}^{3} \sigma_j e^{\kappa_j x}\Psi_j. \tag{2.5}$$

The coefficients σ_j can be determined using the boundary conditions. This procedure is described in detail in [16,37].

Remark 2.1 The solution $\bar{U}_h$ can be written on the form given in (2.5) *unless $s = 0$ at the same time as $v = c$, see Appendix A. In the rest of the paper we assume $v \neq c$.*

Remark 2.2 This technique requires a one-dimensional problem. For problems in multiple dimensions the dimensions tangential to the boundary can be handled by using appropriate expansions, e.g. Fourier transforms (as in [37]) or spherical harmonics, which in turn require an appropriate choice of computational domain.

3 Derivation of the boundary conditions

Before the boundary conditions are constructed it is essential to know how many are needed at each boundary. It is shown in [43,30,16] that for each negative $\mathrm{Re}(\kappa)$ we need one condition at the left boundary, and for each positive $\mathrm{Re}(\kappa)$ we need one condition at the right boundary. The number of roots with negative and positive real parts, respectively, is given by

Proposition 3.1 *Consider the roots of $q(\kappa,s) = 0$ in* (2.4)*. For $v > 0$ and s such that $Re(s) > 0$, two of the κ's have negative real part and one of the κ's has positive real part.*

Proof Assume that κ passes the imaginary axis, i.e. that $\kappa = \beta i$. Inserting this into equation (2.4) and using that $s = \eta + \xi i$ yields

$$c^2\beta^2 + \varepsilon\eta\beta^2 + \eta^2 - (\xi + v\beta)^2 + (2\eta + \varepsilon\beta^2)(\xi + v\beta)i = 0. \tag{3.1}$$

The imaginary part of (3.1) is zero if either $\xi + v\beta = 0$ or $2\eta + \varepsilon\beta^2 = 0$. In both of these cases, it is required that either $\eta < 0$ or that $\eta = \xi = 0$ to cancel the real part. That is, as long as the real part of s is positive ($\eta > 0$), no purely imaginary κ can exist and hence the real part of the κ's can not change sign. Dividing $q(\kappa, s)$ in (2.4) by $-\varepsilon v$ yields

$$\tilde{q}(\kappa,s) = \kappa^3 - \underbrace{\frac{(v^2 - c^2 - s\varepsilon)}{\varepsilon v}}_{r_2}\kappa^2 + \underbrace{\frac{-2s}{\varepsilon}}_{r_1}\kappa - \underbrace{\frac{s^2}{\varepsilon v}}_{r_0} = (\kappa-\kappa_1)(\kappa-\kappa_2)(\kappa-\kappa_3) \tag{3.2}$$

$$r_2 = \kappa_1 + \kappa_2 + \kappa_3, \qquad r_1 = \kappa_1\kappa_2 + \kappa_1\kappa_3 + \kappa_2\kappa_3, \qquad r_0 = \kappa_1\kappa_2\kappa_3,$$

and by assuming s real and large, we get $r_0 > 0$, $r_1 < 0$ and $r_2 < 0$. According to Descartes' rule of signs [39], the polynomial $\tilde{q}(\kappa, s)$ has exactly one positive root for these values of r_0, r_1 and r_2. □

Thus two boundary conditions are needed at the left boundary and one boundary condition is needed at the right boundary, which is a known result for the problem (2.1), see e.g. [31] . Without loss of generality, let $\mathrm{Re}(\kappa_1) < 0$, $\mathrm{Re}(\kappa_2) < 0$ and $\mathrm{Re}(\kappa_3) > 0$. In addition, it holds that

Proposition 3.2 *For $v > 0$ and s such that $Re(s) > 0$, it holds that $Re(\kappa_1/s) < 0$, $Re(\kappa_2/s) < 0$ and $Re(\kappa_3/s) > 0$.*

The proof of Proposition 3.2 is given in Appendix B.

3.1 Non-reflecting boundary conditions

When constructing non-reflecting boundary conditions one prohibits the solution outside the artificial boundary from growing, i.e. $\bar{U}_h(x) \to 0$ as $x \to \pm\infty$ is demanded, see [47]. This is accomplished by canceling the coefficients σ_j in (2.5) corresponding to the growing modes at each boundary.

Remark 3.1 To get an intuitive feeling of the meaning of κ_j, we consider a simplified case. Consider the hyperbolic version of (2.1)*, where the characteristics of $U(x,t)$ travel with constant wave speed a_j. In this case the eigenvalues of the Laplace transformed solution have the form $\kappa_j = -s/a_j$ and the eigenvectors Ψ_j are independent of s, such that*

$$U(x,t) = \sum_j h_j(t - x/a_j)\Psi_j, \qquad \hat{U}(x,s) = \sum_j \hat{h}_j(s)e^{-xs/a_j}\Psi_j.$$

Thus a positive wave speed a_j means that the eigensolution Ψ_j is right-going, and implies that $Re(\kappa_j) = -Re(s)/a_j$ is negative. Likewise, if $Re(\kappa_j) > 0$, the eigenfunction Ψ_j is left-going. For a hyperbolic problem, providing zero data directly to the ingoing variables means that the outgoing waves can pass through the boundary freely, without reflections. Analogously, in (2.5) *we will cancel the modes that are growing outwards, from the computational domain.*

Recall that the real parts of κ_1 and κ_2 are negative and the real part of κ_3 is positive for $\mathrm{Re}(s) > 0$. Our aim is to construct boundary conditions for the left boundary that force σ_1 and σ_2 to zero, and a boundary condition for the right boundary that forces σ_3 to zero. With access to the eigenvalues κ_i (they will be computed numerically for each s) we compute the eigenvectors Ψ_i and the corresponding orthogonal vector Φ_i

$$\Psi_i = \begin{bmatrix} -c \\ (s+v\kappa_i)/\kappa_i \\ s+v\kappa_i \end{bmatrix}, \qquad \Phi_i = \begin{bmatrix} \varepsilon(v\kappa_j+s)(v\kappa_k+s)/sc \\ \varepsilon v\kappa_j\kappa_k/s \\ \varepsilon \end{bmatrix}, \tag{3.3}$$

where κ_j and κ_k are the remaining two roots (if $\kappa_i = \kappa_1$ then $\kappa_{j,k} = \kappa_{2,3}$). The vector Φ_l is orthogonal to Ψ_i for $i \neq l$, such that

$$\Phi_i^T\Psi_i = \varepsilon v(\kappa_i-\kappa_j)(\kappa_i-\kappa_k)/\kappa_i, \qquad \Phi_j^T\Psi_i = 0, \qquad \Phi_k^T\Psi_i = 0. \tag{3.4}$$

Using (2.5) and (3.4) we see that the boundary condition $\Phi_i^T\bar{U}_h = 0$ is equivalent to $\sigma_i e^{\kappa_i x}\Phi_i^T\Psi_i = 0$, which forces σ_i to zero. This gives the exact non-reflecting boundary conditions

$$x = x_L: \quad \begin{cases} \Phi_1^T\bar{U}_h = 0 \\ \Phi_2^T\bar{U}_h = 0 \end{cases}, \qquad x = x_R: \quad \Phi_3^T\bar{U}_h = 0. \tag{3.5}$$

The boundary conditions (3.5) are $\bar{L}_L\bar{U}_h = 0$ and $\bar{L}_R\bar{U}_h = 0$, where

$$\bar{L}_L = [\Phi_1,\ \Phi_2]^T, \qquad \bar{L}_R = \Phi_3^T. \tag{3.6}$$

Thus we can identify the data in (2.3), as

$$\bar{L}_{L,R}\bar{U} = \bar{L}_{L,R}(\bar{U}_h+\bar{U}_p) = \bar{L}_{L,R}\bar{U}_p \qquad \Longrightarrow \qquad \hat{g}_{L,R} = \bar{L}_{L,R}\bar{U}_p.$$

Finding the data $\hat{g}_{L,R}$ can be difficult. Common choices are to assume that $\bar{U}_p$ is constant or zero. To take the (non-optimal) possibility of inaccurate data into account, assume that the boundary data has been chosen such that $\hat{g}_{L,R} = \bar{L}_{L,R}\bar{U}_p + g'_{L,R}$. Then, in practice, the boundary conditions imposed are

$$x = x_L: \quad \bar{L}_L\bar{U}_h = g'_L, \qquad x = x_R: \quad \bar{L}_R\bar{U}_h = g'_R, \tag{3.7}$$

where $g'_{L,R}$ are perturbations close to (or preferably equal to) zero.

Remark 3.2 The particular solution $\bar{U}_p$ depends on $\bar{F}$, which in turn depends on the forcing function F and the initial function f in (2.1)*. Often these functions are defined so that they have compact support, which implies that $\bar{U}_p = 0$ at the boundaries and that $\hat{g}_{L,R} = 0$.*

3.2 The resulting boundary operators

The boundary operators in (3.6) can be written

$$\bar{L}_L = \begin{bmatrix} \alpha_1 & \beta_1 & \varepsilon \\ \alpha_2 & \beta_2 & \varepsilon \end{bmatrix}, \qquad \bar{L}_R = \begin{bmatrix} \alpha_3 & \beta_3 & \varepsilon \end{bmatrix}, \tag{3.8}$$

where α_j, β_j depend on s and $\kappa_j(s)$. The structure of the complementing vectors in (3.3) and the relations in (3.2) gives

$$\alpha_i = \frac{-sc}{s+v\kappa_i}, \qquad\qquad \beta_i = \frac{s}{\kappa_i}.$$

The operators in (3.8) are suitable for the problem formulation in (2.3) but can also be rewritten such that they are appropriate for the problem (2.2), as

$$\begin{aligned} \hat{L}_L\hat{U} &= H_L\hat{U} + G_L\hat{U}_x = \hat{g}_L, \qquad H_L = \begin{bmatrix} \alpha_1 & \beta_1 \\ \alpha_2 & \beta_2 \end{bmatrix}, \qquad G_L = \begin{bmatrix} 0 & \varepsilon \\ 0 & \varepsilon \end{bmatrix}, \\ \hat{L}_R\hat{U} &= H_R\hat{U} + G_R\hat{U}_x = \hat{g}_R, \qquad H_R = \begin{bmatrix} \alpha_3 & \beta_3 \end{bmatrix}, \qquad G_R = \begin{bmatrix} 0 & \varepsilon \end{bmatrix}. \end{aligned} \tag{3.9}$$

3.3 The boundary operators in the hyperbolic limit

In the limit $\varepsilon \to 0$ the problem (2.1) becomes hyperbolic. From (2.4) we can see that the determinant will be reduced to a second order polynomial in κ, with two roots. Since the determinant can be rescaled such that κ/s is a function of εs, see Appendix B, the Taylor expansion for small ε is the same as for small s. Thus the two roots in the hyperbolic case will correspond to κ_2 and κ_3 (since $\kappa_1 \to -\infty$ as $\varepsilon \to 0$), see Appendix A.1, and the operators in (3.9) become

$$\begin{aligned} H_L &= -(v+c)\begin{bmatrix} 0 & 0 \\ 1 & 1 \end{bmatrix}, \qquad G_L = \begin{bmatrix} 0 & 0 \\ 0 & 0 \end{bmatrix}, \\ H_R &= (v-c)\begin{bmatrix} 1 & -1 \end{bmatrix}, \qquad G_R = \begin{bmatrix} 0 & 0 \end{bmatrix}. \end{aligned} \tag{3.10}$$

Note that the first rows of H_L and G_L are equal to zero, which implies that only one boundary condition will be given at the left boundary. Note also that we have here assumed that $v < c$. For $v > c$ we would instead get two boundary conditions at the left boundary and none at the right boundary.

4 Well-posedness of the IBVP

A problem is well-posed (Hadamard's well-posedness) if: i) A solution exists, ii) The solution is unique, iii) The solution depends continuously on (and is bounded by) provided data. Existence is guaranteed by using the right number of boundary conditions and uniqueness follows from iii). We will focus on the third requirement, which is equivalent to limit the growth of the solution, see [16].

The problem (2.1) is well-posed if there does not exist any solution $U(x,t)$ that grow exponentially in time, see for example [30,16,17,31]. If a problem is well-posed in this particular sense, it has a negative spectrum and will fulfill the Kreiss condition, see below. (A more generous definition of well-posedness, that opens up for a wider range of problems, is to accept bounded growth of the solution. In this paper we limit ourselves to zero growth.)

4.1 Well-posedness in the sense of Kreiss

Consider the homogeneous solution (2.5). By defining

$$\Psi = [\Psi_1, \Psi_2, \Psi_3], \qquad K(x) = diag(e^{\kappa_1 x},\, e^{\kappa_2 x},\, e^{\kappa_3 x}), \qquad \sigma = [\sigma_1, \sigma_2, \sigma_3]^T,$$

we can write $\bar{U}_h = \Psi K \sigma$. Next, the boundary conditions in (3.7) are applied, yielding

$$E(s)\sigma = g', \quad E(s) = \begin{bmatrix} \bar{L}_L \Psi K(x_L) \\ \bar{L}_R \Psi K(x_R) \end{bmatrix} = \begin{bmatrix} e^{\kappa_1 x_L} \Phi_1^T \Psi_1 & e^{\kappa_2 x_L} \Phi_1^T \Psi_2 & e^{\kappa_3 x_L} \Phi_1^T \Psi_3 \\ e^{\kappa_1 x_L} \Phi_2^T \Psi_1 & e^{\kappa_2 x_L} \Phi_2^T \Psi_2 & e^{\kappa_3 x_L} \Phi_2^T \Psi_3 \\ e^{\kappa_1 x_R} \Phi_3^T \Psi_1 & e^{\kappa_2 x_R} \Phi_3^T \Psi_2 & e^{\kappa_3 x_R} \Phi_3^T \Psi_3 \end{bmatrix},$$

where $g' = [(g'_L)^T, (g'_R)^T]^T$. Each row of the system above corresponds to one boundary condition, and for general boundary conditions the matrix $E(s)$ is full. If $E(s)$ is non-singular we can solve for σ and obtain a unique solution $\bar{U} = \bar{U}_p + \Psi K E(s)^{-1} g'$. Recalling that the first two entries of $\bar{U}$ are denoted $\hat{U}$, we can formally transform back to the time domain, as

$$U(x,t) = \mathscr{L}^{-1}\{\hat{U}\} = e^{\eta_0 t} \left(\frac{1}{2\pi} \int_{-\infty}^{+\infty} \hat{U}(x, \eta_0 + i\xi) e^{i\xi t} d\xi \right)$$

where $E(s)$ must be non-singular for $\eta \geq \eta_0$.

Definition 4.1 The problem (2.1) is well-posed in the sense of Kreiss if $|E(s)| \neq 0$ holds for $\mathrm{Re}(s) \geq 0$, see [16], i.e. if $\eta_0 \leq 0$.

The Kreiss condition is a stronger version of the Lopatinskii condition, see [16, 11,31].

Proposition 4.1 *Consider the ordinary differential equation* (2.3) *with boundary operators* (3.6)*. For $v > 0$, $v \neq c$ the corresponding matrix $E(s)$ satisfies the Kreiss condition, and hence the problem* (2.1) *is well-posed in the sense of Definition 4.1.*

Proof Using that $\Phi_j^T \Psi_i = 0$ for $i \neq j$ leads to

$$E(s) = \begin{bmatrix} e^{\kappa_1 x_L} \Phi_1^T \Psi_1 & 0 & 0 \\ 0 & e^{\kappa_2 x_L} \Phi_2^T \Psi_2 & 0 \\ 0 & 0 & e^{\kappa_3 x_R} \Phi_3^T \Psi_3 \end{bmatrix}.$$

From (3.4) we know that $\Phi_i^T \Psi_i = \varepsilon v (\kappa_i - \kappa_j)(\kappa_i - \kappa_k)/\kappa_i$ and thereby the three entries of $E(s)$ are non-zero if the roots κ_i, κ_j, κ_k are distinct. In Appendix A it is shown that there are no multiple roots for $\mathrm{Re}(s) \geq 0$, unless $s = 0$. This special case is treated separately in Appendix A.1, where it is shown that $\lim_{s\to 0} \Phi_j^T \Psi_j \neq 0$ as long as $v \neq c$. Consequently $|E(s)| \neq 0$ for all $\mathrm{Re}(s) \geq 0$ when $v \neq c$. □

Remark 4.1 Well-posedness in the sense of Definition 4.1 states that the solution does not have exponential growth in time (if $\eta_0 \leq 0$). The same holds for the energy norm of the solution, and hence this well-posedness result leads to the existence of an energy estimate.

4.2 Well-posedness in the energy sense

Next we show that the non-reflecting boundary conditions also lead to an energy estimate (which is guaranteed, as stated in Remark 4.1). We will do this by showing that the homogenous solution $\hat{U}_h$ is bounded using the energy method. The homogenous version of equation (2.2) is multiplied by the conjugate transpose of $\hat{U}_h$ (denoted $\hat{U}_h^*$) from the left and integrated with respect to x. Adding the complex conjugate of the resulting relation to itself, and using that $s = \eta + \xi i$, we get

$$2\eta \int_{x_L}^{x_R} \hat{U}_h^* \hat{U}_h dx + 2 \int_{x_L}^{x_R} (\hat{U}_h)_x^* B (\hat{U}_h)_x dx = BT_L + BT_R \tag{4.1}$$

where

$$BT_L = \hat{U}_h^* A \hat{U}_h - \hat{U}_h^* B (\hat{U}_h)_x - (\hat{U}_h)_x^* B \hat{U}_h \big|_{x_L}, \quad BT_R = -\hat{U}_h^* A \hat{U}_h + \hat{U}_h^* B (\hat{U}_h)_x + (\hat{U}_h)_x^* B \hat{U}_h \big|_{x_R}. \tag{4.2}$$

We know from the previous analysis of $E(s)$ that the operators in (3.6) give a well-posed problem. However, if the boundary conditions can be imposed such that the boundary terms BT_L and BT_R are non-positive, we obtain an energy estimate which will lead directly to stability of the discrete problem.

Since we have derived the boundary conditions for the first order form in (2.3) we rewrite (4.2) on the equivalent form

$$BT_L = \bar{U}_h^* \widetilde{A} \bar{U}_h \Big|_{x_L}, \qquad BT_R = -\bar{U}_h^* \widetilde{A} \bar{U}_h \Big|_{x_R}, \qquad \widetilde{A} = \begin{bmatrix} v & c & 0 \\ c & v & -\varepsilon \\ 0 & -\varepsilon & 0 \end{bmatrix}. \tag{4.3}$$

Proposition 4.2 *The left boundary term in* (4.3) *is non-positive, i.e.* $BT_L \leq 0$.

Proof The left boundary conditions in (3.5) force σ_1 and σ_2 to zero which yields the solution $\bar{U}_h = \sigma_3 e^{\kappa_3 x} \Psi_3$. Inserting this into (4.3) we obtain $BT_L = |\sigma_3 e^{\kappa_3 x_L}|^2 \mathscr{A}_L$ where

$$\mathscr{A}_L = \Psi_3^* \widetilde{A} \Psi_3 = -\mathrm{Re}\left(\frac{s}{\kappa_3}\right)\left(c^2 + \left|\frac{s + v\kappa_3}{\kappa_3}\right|^2\right) - \varepsilon \mathrm{Re}\,(\kappa_3) \left|\frac{s+v\kappa_3}{\kappa_3}\right|^2 \leq 0. \tag{4.4}$$

In the last inequality we used that $\mathrm{Re}(\kappa_3/s) > 0$ and $\mathrm{Re}(\kappa_3) > 0$ for $\mathrm{Re}(s) > 0$, see Proposition 3.1 and Proposition 3.2. For details on the derivation of (4.4) see Appendix C. □

Proposition 4.3 *The right boundary term in* (4.3) *is non-positive, i.e.*$BT_R \leq 0$.

The proof of Proposition 4.3 is given in Appendix C.1 and results in

$$BT_R = -\begin{bmatrix}\sigma_1 e^{\kappa_1 x_R}\\ \sigma_2 e^{\kappa_2 x_R}\end{bmatrix}^* \mathscr{A}_R \begin{bmatrix}\sigma_1 e^{\kappa_1 x_R}\\ \sigma_2 e^{\kappa_2 x_R}\end{bmatrix}, \qquad \mathscr{A}_R = \begin{bmatrix}\Psi_1^* \widetilde{A}\Psi_1 & \Psi_1^* \widetilde{A}\Psi_2\\ \Psi_2^* \widetilde{A}\Psi_1 & \Psi_2^* \widetilde{A}\Psi_2\end{bmatrix} \geq 0. \tag{4.5}$$

Since the boundary terms BT_L and BT_R are non-positive, the right hand side of (4.1) is bounded, which leads to $\eta \leq 0$ and an energy estimate. We have assumed that the solution is in L^2, and hence boundedness of the transformed solution $\hat{U}$ leads to boundedness of U, via the Plancherel theorem, see [31].

In the proofs of Proposition 4.2 and Proposition 4.3 we have assumed that the provided data is exact, such that $\sigma_{1,2} = 0$ at the left boundary or $\sigma_3 = 0$ at the right boundary. In Sect. 6 we will also include the possibility of having non-zero (incorrect) boundary data and show that the problem is in fact strongly well-posed.

A derivation of NRBC's similar to the one presented in Section 3 above, can be found in [48] for a parabolic system and a system of Schrödinger-type. In [48], a corresponding derivation of NRBC's for the discrete problem is also performed. Here we instead continue by discretizing the derived problem directly.

5 The semi-discrete problem formulation

Next, we will derive the semi-discrete problem formulation. We employ a finite difference method to approximate the space differentiation, and the difference operators are on so called summation by parts (SBP) form. Further, the boundary conditions are implemented using penalty terms, a technique also known as weak boundary implementation or as the simultaneous approximation term (SAT) technique. For a read-up on SBP and SAT, see [46] and references therein.

5.1 The numerical scheme

Consider our original problem (2.1). The domain $x \in [x_L, x_R]$ is discretized in space using $N+1$ equidistant grid points, as $x_i = x_L + (x_R - x_L)i/N$, where $i = 0, 1, \ldots, N$. The solution U is represented by a discrete solution vector V of length $2(N+1)$, such that $V = [V_0^T, V_1^T, \ldots, V_N^T]^T$ where $V_i(t) \approx U(x_i, t)$. The semi-discrete scheme for the IBVP in (2.1) is then written

$$\begin{aligned} V_t + (D \otimes A)V - (D^2 \otimes B)V &= F + ((\Sigma_0 * V)(t) - \Gamma_0) + ((\Sigma_N * V)(t) - \Gamma_N), \\ V(0) &= f, \end{aligned} \tag{5.1}$$

where the symbol $\otimes$ refers to the Kronecker product, and the symbol $*$ refers to the convolution operation. The boundary conditions (3.9) are imposed weakly in (5.1) using the SAT technique, by the penalty terms $((\Sigma_{0,N} * V)(t) - \Gamma_{0,N}(t))$ which are yet unknown but will be derived in the Laplace transformed domain. Further, the difference operator D (which mimics $\partial/\partial x$) is on SBP form, and hence the following holds

$$D = P^{-1}Q, \qquad Q + Q^T = e_N e_N^T - e_0 e_0^T, \qquad P = P^T > 0, \tag{5.2}$$

where $e_0 = [1,0,\dots,0]^T$ and $e_N = [0,\dots,0,1]^T$. Typical examples of P and Q can be found in [42, 7]. The second derivative $\partial^2/\partial x^2$ is approximated by the wide operator D^2. Note that we use the same notation for F, f both in the continuous and the discrete setting.

Analogously to the continuous case, stability will be shown in the Laplace transformed space. By Laplace transforming (5.1) the discrete representation of (2.2) is obtained, as

$$s\hat{V} + (D\otimes A)\hat{V} - (D^2\otimes B)\hat{V} = \hat{F} + f + \left(\hat{\Sigma}_0\hat{V} - \hat{\Gamma}_0\right) + \left(\hat{\Sigma}_N\hat{V} - \hat{\Gamma}_N\right), \tag{5.3}$$

where $\hat{V}(s) = \mathscr{L}\{V(t)\}$ and where $\hat{\Sigma}_{0,N}$, $\hat{\Gamma}_{0,N}$ remains to be determined. As in the continuous case we omit the forcing function $\hat{F} + f$. We multiply (5.3) by $\hat{V}^*\bar{P}$ from the left, where $\bar{P} = P\otimes I_2$, and add the conjugate transpose of the equation to itself. Thereafter using the SBP-properties in (5.2) yields

$$2\eta\hat{V}^*\bar{P}\hat{V} + 2(\bar{D}\hat{V})^*(P\otimes B)\bar{D}\hat{V} = BT_L^D + BT_R^D, \tag{5.4}$$

where $\bar{D} = D\otimes I_2$ and where

$$\begin{aligned} BT_L^D &= \hat{V}_0^*A\hat{V}_0 - \hat{V}_0^*B(\bar{D}\hat{V})_0 - (\bar{D}\hat{V})_0^*B\hat{V}_0 \\ &\quad + \hat{V}^*\bar{P}(\hat{\Sigma}_0\hat{V} - \hat{\Gamma}_0) + (\hat{\Sigma}_0\hat{V} - \hat{\Gamma}_0)^*\bar{P}\hat{V} \\ BT_R^D &= -\hat{V}_N^*A\hat{V}_N + \hat{V}_N^*B(\bar{D}\hat{V})_N + (\bar{D}\hat{V})_N^*B\hat{V}_N \\ &\quad + \hat{V}^*\bar{P}(\hat{\Sigma}_N\hat{V} - \hat{\Gamma}_N) + (\hat{\Sigma}_N\hat{V} - \hat{\Gamma}_N)^*\bar{P}\hat{V}. \end{aligned} \tag{5.5}$$

Note the similarity between the semi-discrete energy growth rate (5.4) and the continuous one in (4.1).

The matrices $\hat{\Sigma}_{0,N}$ and the vectors $\hat{\Gamma}_{0,N}$ depend on how the boundary conditions are imposed. We use the following ansätze for the penalty terms

$$\begin{aligned} \hat{\Sigma}_0\hat{V} - \hat{\Gamma}_0 &= (P^{-1}e_0\otimes\tau_0 + P^{-1}D^Te_0\otimes\sigma_0)(H_L\hat{V}_0 + G_L(\bar{D}\hat{V})_0 - \hat{g}_L) \\ \hat{\Sigma}_N\hat{V} - \hat{\Gamma}_N &= (P^{-1}e_N\otimes\tau_N + P^{-1}D^Te_N\otimes\sigma_N)(H_R\hat{V}_N + G_R(\bar{D}\hat{V})_N - \hat{g}_R), \end{aligned} \tag{5.6}$$

where the boundary operators $H_{L,R}$, $G_{L,R}$ are given in (3.9). The penalty parameters $\tau_{0,N}$, $\sigma_{0,N}$ (where τ_0 and σ_0 are 2×2 matrices and τ_N and σ_N are 2×1 vectors) will be determined in the next section. Note that all dependence of boundary data sits in $\hat{\Gamma}_{0,N}$, such that $\hat{\Gamma}_{0,N} = 0$ if $\hat{g}_{L,R} = 0$. By inserting the expressions (5.6) into (5.5), the boundary terms can be written as

$$\begin{aligned} BT_L^D = &\begin{bmatrix}\hat{V}_0\\(\bar{D}\hat{V})_0\end{bmatrix}^*\begin{bmatrix}A+\tau_0H_L+(\tau_0H_L)^* & -B+\tau_0G_L+(\sigma_0H_L)^*\\ -B+\sigma_0H_L+(\tau_0G_L)^* & \sigma_0G_L+(\sigma_0G_L)^*\end{bmatrix}\begin{bmatrix}\hat{V}_0\\(\bar{D}\hat{V})_0\end{bmatrix} \\ &-\begin{bmatrix}\hat{V}_0\\(\bar{D}\hat{V})_0\end{bmatrix}^*\begin{bmatrix}\tau_0\\\sigma_0\end{bmatrix}\hat{g}_L - \left(\begin{bmatrix}\hat{V}_0\\(\bar{D}\hat{V})_0\end{bmatrix}^*\begin{bmatrix}\tau_0\\\sigma_0\end{bmatrix}\hat{g}_L\right)^* \end{aligned} \tag{5.7}$$

and

$$\begin{aligned} BT_R^D = &\begin{bmatrix}\hat{V}_N\\(\bar{D}\hat{V})_N\end{bmatrix}^*\begin{bmatrix}-A+\tau_NH_R+(\tau_NH_R)^* & B+\tau_NG_R+(\sigma_NH_R)^*\\ B+\sigma_NH_R+(\tau_NG_R)^* & \sigma_NG_R+(\sigma_NG_R)^*\end{bmatrix}\begin{bmatrix}\hat{V}_N\\(\bar{D}\hat{V})_N\end{bmatrix} \\ &-\begin{bmatrix}\hat{V}_N\\(\bar{D}\hat{V})_N\end{bmatrix}^*\begin{bmatrix}\tau_N\\\sigma_N\end{bmatrix}\hat{g}_R - \left(\begin{bmatrix}\hat{V}_N\\(\bar{D}\hat{V})_N\end{bmatrix}^*\begin{bmatrix}\tau_N\\\sigma_N\end{bmatrix}\hat{g}_R\right)^*, \end{aligned} \tag{5.8}$$

respectively.

Similarly to the definition of well-posedness for the continuous problem, a numerical scheme is energy stable if the growth of the solution is bounded. As in the continuous case we limit ourselves to zero growth, which means that $\eta \leq 0$ in (5.4) is needed. Hence, to prove stability, we must show that the boundary terms in (5.7) and (5.8) are non-positive for zero data. In the next section, we show how to choose the penalty parameters $\tau_{0,N}$ and $\sigma_{0,N}$ such that $BT^D_{L,R} \leq 0$.

Remark 5.1 As mentioned, in the next section we will show that the penalty parameters can be chosen such that the discrete boundary terms mimics the continuous ones, see Propositions 6.3 and 6.4. This is manageable because of the summation by part properties of our numerical method. However, the procedure presented here is of course not limited to finite differences methods, but is feasible also with various Galerkin or discontinuous Galerkin techniques where the discrete energy estimate mimics the continuous energy estimate, e.g. the discontinuous Galerkin collocation spectral element method in [29].

6 Energy estimates in Laplace space

The penalty parameters $\tau_{0,N}$ and $\sigma_{0,N}$ in (5.6) are not uniquely determined from the stability requirements. The strategy is to first reformulate the continuous boundary terms $BT_{L,R}$ using the boundary conditions, and then to choose the penalty parameters such that the discrete boundary terms $BT^D_{L,R}$ mimic the continuous ones. This can be done in several ways, of which we will present one here. See [10] for an alternative formulation.

6.1 The continuous boundary terms

Consider the matrix $\widetilde{A}$ in (4.3), and assume that we have found a rotation such that $\widetilde{A} = X\Lambda X^T$, where Λ is diagonal. Note that the elements of Λ are not necessarily the eigenvalues of $\widetilde{A}$, and that the vectors in X may then not be orthogonal. According to Sylvester's law of inertia, the matrices $\widetilde{A}$ and Λ will always have the same number of positive/negative eigenvalues for a non-singular X. The matrix Λ has two positive entries and one negative entry for $v > 0$, and is sorted as $\Lambda = diag(\Lambda_+, \Lambda_-)$. The vectors are divided correspondingly, $X = [x_+, x_-]$, and the boundary terms in (4.3) are rewritten as

$$\begin{aligned} BT_L &= \quad (X^T\bar{U})^*\Lambda X^T\bar{U}\big|_{x_L} = \quad (x_+^T\bar{U})^*\Lambda_+ x_+^T\bar{U} + (x_-^T\bar{U})^*\Lambda_- x_-^T\bar{U}\big|_{x_L} \\ BT_R &= -(X^T\bar{U})^*\Lambda X^T\bar{U}\big|_{x_R} = -(x_+^T\bar{U})^*\Lambda_+ x_+^T\bar{U} - (x_-^T\bar{U})^*\Lambda_- x_-^T\bar{U}\big|_{x_R}. \end{aligned} \tag{6.1}$$

$x_+^T\bar{U}$ represents two right-going variables (ingoing at the left boundary), and $x_-^T\bar{U}$ represents one left-going variable (ingoing at the right boundary). The ingoing variables are given data in terms of known functions and outgoing variables, as

$$x = x_L: \quad x_+^T\bar{U} + R_L x_-^T\bar{U} = \tilde{g}_L, \qquad x = x_R: \quad x_-^T\bar{U} + R_R x_+^T\bar{U} = \tilde{g}_R, \tag{6.2}$$

where the matrices $R_{L,R}$ must be sufficiently small. Since we want to impose the non-reflecting boundary conditions $\bar{L}_L\bar{U} = \hat{g}_L$ and $\bar{L}_R\bar{U} = \hat{g}_R$, given in (2.3), we relate them to the general ones in (6.2) using scaling matrices. Denoting the scaling matrices $J_{L,R}$, we obtain

$$\bar{L}_L = J_L(x_+^T + R_L x_-^T), \qquad \bar{L}_R = J_R(x_-^T + R_R x_+^T), \tag{6.3}$$

and identify $\tilde{g}_L = J_L^{-1}\hat{g}_L$ and $\tilde{g}_R = J_R^{-1}\hat{g}_R$. The matrices $J_{L,R}$ and $R_{L,R}$ can be computed from $\bar{L}_{L,R}$, which are given in (3.8), and $x_\pm$. Inserting the relations $x_+^T\bar{U} = \tilde{g}_L - R_L x_-^T\bar{U}$ and $x_-^T\bar{U} = \tilde{g}_R - R_R x_+^T\bar{U}$ from (6.2), into the boundary terms BT_L and BT_R in (6.1), respectively, yields

$$\begin{aligned} BT_L = & \left(x_-^T\bar{U} - \mathscr{C}_L^{-1}R_L^*\Lambda_+\tilde{g}_L\right)^* \mathscr{C}_L \left(x_-^T\bar{U} - \mathscr{C}_L^{-1}R_L^*\Lambda_+\tilde{g}_L\right)\Big|_{x_L} \\ & + \tilde{g}_L^*\left(\Lambda_+ - \Lambda_+R_L\mathscr{C}_L^{-1}R_L^*\Lambda_+\right)\tilde{g}_L \\ BT_R = & -\left(x_+^T\bar{U} - \mathscr{C}_R^{-1}R_R^*\Lambda_-\tilde{g}_R\right)^* \mathscr{C}_R \left(x_+^T\bar{U} - \mathscr{C}_R^{-1}R_R^*\Lambda_-\tilde{g}_R\right)\Big|_{x_R} \\ & - \tilde{g}_R^*(\Lambda_- - \Lambda_-R_R\mathscr{C}_R^{-1}R_R^*\Lambda_-)\tilde{g}_R \end{aligned} \tag{6.4}$$

where $\mathscr{C}_L = R_L^*\Lambda_+R_L + \Lambda_-$ and $\mathscr{C}_R = \Lambda_+ + R_R^*\Lambda_-R_R$. For an energy estimate of the continuous problem $\mathscr{C}_L \le 0$ and $\mathscr{C}_R \ge 0$ are necessary.

Proposition 6.1 *The scalar $\mathscr{C}_L$ in* (6.4) *is non-positive, and hence the non-reflecting boundary condition* (3.7) *at the left boundary leads to an energy estimate.*

Proof Recall that $\widetilde{A} = x_+\Lambda_+x_+^T + x_-\Lambda_-x_-^T$ and that $\bar{L}_L = [\Phi_1,\ \Phi_2]^T$ and $\Phi_j^T\Psi_i = 0$ for $i \neq j$ such that $\bar{L}_L\Psi_3 = 0$. Starting from $\mathscr{A}_L$ in (4.4), we have

$$\begin{aligned} \mathscr{A}_L &= \Psi_3^*\widetilde{A}\Psi_3 \\ &= \Psi_3^*\left((J_L^{-1}\bar{L}_L - R_Lx_-^T)^*\Lambda_+(J_L^{-1}\bar{L}_L - R_Lx_-^T) + x_-\Lambda_-x_-^T\right)\Psi_3 \\ &= \Psi_3^*x_-\mathscr{C}_Lx_-^T\Psi_3, \end{aligned}$$

where we used the relation $x_+^T = J_L^{-1}\bar{L}_L - R_Lx_-^T$ from (6.3) in the first step. In the last step we used that $\bar{L}_L\Psi_3 = 0$. We thus have the relation $\mathscr{A}_L = (x_-^T\Psi_3)^*\mathscr{C}_Lx_-^T\Psi_3$, where $x_-^T\Psi_3 \neq 0$, and since we know from Proposition 4.2 that $\mathscr{A}_L \le 0$ we also know that $\mathscr{C}_L \le 0$. □

Proposition 6.2 *The matrix $\mathscr{C}_R$ in* (6.4) *is non-negative, and hence the non-reflecting boundary condition* (3.7) *at the right boundary leads to an energy estimate.*

Proof Recall that $\bar{L}_R = \Phi_3^T$ and that $\Phi_j^T\Psi_i = 0$ for $i \neq j$. This makes $\bar{L}_R\Psi_1 = 0$ and $\bar{L}_R\Psi_2 = 0$. Denoting the components of $\mathscr{A}_R$ in (4.5) as $\mathscr{A}_R^{ji}$, where $i = 1,2$ and $j = 1,2$, gives

$$\begin{aligned} \mathscr{A}_R^{ji} &= \Psi_j^*\widetilde{A}\Psi_i \\ &= \Psi_j^*\left(x_+\Lambda_+x_+^T + (J_R^{-1}\bar{L}_R - R_Rx_+^T)^*\Lambda_-(J_R^{-1}\bar{L}_R - R_Rx_+^T)\right)\Psi_i \\ &= \Psi_j^*x_+\mathscr{C}_Rx_+^T\Psi_i, \end{aligned}$$

where the relation $x_-^T = J_R^{-1}\bar{L}_R - R_R x_+^T$ from (6.3) was used in the first step. In the last step we used that $\bar{L}_R\Psi_i = 0$ for $i = 1,2$. From these coefficients we compose

$$\mathscr{A}_R = \left(x_+^T\left[\,\Psi_1\ \Psi_2\,\right]\right)^* \mathscr{C}_R x_+^T\left[\,\Psi_1\ \Psi_2\,\right],$$

where $x_+^T[\Psi_1\ \Psi_2]$ is a non-singular 2×2 matrix. Since $\mathscr{A}_R \geq 0$ from Proposition 4.3, we know that $\mathscr{C}_R \geq 0$. □

Remark 6.1 In the proofs above $x_-^T\Psi_3$ and $x_+^T[\Psi_1\ \Psi_2]$ must be non-singular. By combining $\bar{L}_L\Psi_3 = 0$, $\bar{L}_R\Psi_{1,2} = 0$ together with (6.3) *it is possible to write*

$$X^T\Psi = \begin{bmatrix} I_2 & -R_L \\ -R_R & 1 \end{bmatrix}\begin{bmatrix} x_+^T[\Psi_1\ \Psi_2] & 0_{2,1} \\ 0_{1,2} & x_-^T\Psi_3 \end{bmatrix}$$

and we see that they are indeed non-singular, since neither X nor Ψ is singular.

6.2 The discrete boundary terms

The continuous boundary terms in (6.1) depend on $\bar{U} = [\hat{p}, \hat{u}, \hat{u}_x]^T$, while the discrete boundary terms in equation (5.7) and (5.8) depend on $\hat{V}_j = [\hat{p}_j, \hat{u}_j]^T$ and $(\bar{D}\hat{V})_j = [(D\hat{p})_j, (D\hat{u})_j]^T$, ($j$ being 0 or N). The additional dependence on $(D\hat{p})_0$ and $(D\hat{p})_N$ will be removed. The penalty parameters are

$$\tau_0 = \begin{bmatrix} \tau_0^{11} & \tau_0^{12} \\ \tau_0^{21} & \tau_0^{22} \end{bmatrix}, \quad \sigma_0 = \begin{bmatrix} \sigma_0^{11} & \sigma_0^{12} \\ \sigma_0^{21} & \sigma_0^{22} \end{bmatrix}, \quad \tau_N = \begin{bmatrix} \tau_N^{11} \\ \tau_N^{21} \end{bmatrix}, \quad \sigma_N = \begin{bmatrix} \sigma_N^{11} \\ \sigma_N^{21} \end{bmatrix}. \tag{6.5}$$

Zeroing out the first row of $\sigma_{0,N}$ such that $\sigma_0^{11} = \sigma_0^{12} = 0$ and $\sigma_N^{11} = 0$, the boundary terms in (5.7) and (5.8) become independent on $(D\hat{p})_0$ and $(D\hat{p})_N$, respectively. Denoting the remaining rows $\tilde{\sigma}_0 = [\sigma_0^{21}, \sigma_0^{22}]$ and $\tilde{\sigma}_N = [\sigma_N^{21}]$, the boundary terms in (5.7) and (5.8) can be written

$$BT_L^D = \bar{V}_0^*\left[\widetilde{A} + \begin{bmatrix} \tau_0 \\ \tilde{\sigma}_0 \end{bmatrix}\bar{L}_L + \bar{L}_L^*\begin{bmatrix} \tau_0 \\ \tilde{\sigma}_0 \end{bmatrix}^*\right]\bar{V}_0 - \bar{V}_0^*\begin{bmatrix} \tau_0 \\ \tilde{\sigma}_0 \end{bmatrix}\hat{g}_L - \hat{g}_L^*\begin{bmatrix} \tau_0 \\ \tilde{\sigma}_0 \end{bmatrix}^*\bar{V}_0 \tag{6.6}$$

$$BT_R^D = \bar{V}_N^*\left[-\widetilde{A} + \begin{bmatrix} \tau_N \\ \tilde{\sigma}_N \end{bmatrix}\bar{L}_R + \bar{L}_R^*\begin{bmatrix} \tau_N \\ \tilde{\sigma}_N \end{bmatrix}^*\right]\bar{V}_N - \bar{V}_N^*\begin{bmatrix} \tau_N \\ \tilde{\sigma}_N \end{bmatrix}\hat{g}_R - \hat{g}_R^*\begin{bmatrix} \tau_N \\ \tilde{\sigma}_N \end{bmatrix}^*\bar{V}_N, \tag{6.7}$$

where $\bar{V}_0 = [\hat{p}_0, \hat{u}_0, (D\hat{u})_0]^T$ and $\bar{V}_N = [\hat{p}_N, \hat{u}_N, (D\hat{u})_N]^T$.

Proposition 6.3 *Choosing the penalty parameter elements τ_0^{ij} and σ_0^{ij} in* (6.5) *as*

$$\sigma_0^{11} = \sigma_0^{12} = 0, \qquad \begin{bmatrix} \tau_0^{11} & \tau_0^{12} \\ \tau_0^{21} & \tau_0^{22} \\ \sigma_0^{21} & \sigma_0^{22} \end{bmatrix} = -x_+\Lambda_+ J_L^{-1}$$

results in a strongly stable numerical scheme.

Proof Inserting the specific choice $[\tau_0^T,\ \tilde{\sigma}_0^T]^T = -x_+\Lambda_+\bar{J}_L^{-1}$ into (6.6) yields

$$\begin{aligned} BT_L^D = &\left(x_-^T\bar{V}_0 - \mathscr{C}_L^{-1}R_L^*\Lambda_+\tilde{g}_L\right)^*\mathscr{C}_L\left(x_-^T\bar{V}_0 - \mathscr{C}_L^{-1}R_L^*\Lambda_+\tilde{g}_L\right) \\ &+\tilde{g}_L^*\left(\Lambda_+ - \Lambda_+R_L\mathscr{C}_L^{-1}R_L^*\Lambda_+\right)\tilde{g}_L - (\bar{L}_L\bar{V}_0 - \hat{g}_L)^*J_L^{-*}\Lambda_+J_L^{-1}(\bar{L}_L\bar{V}_0 - \hat{g}_L) \end{aligned} \tag{6.8}$$

where, according to Proposition 6.1, $\mathscr{C}_L \leq 0$. □

Proposition 6.4 *Choosing the penalty parameter elements τ_N^{ij} and σ_N^{ij} in* (6.5) *as*

$$\sigma_N^{11} = 0, \qquad \begin{bmatrix} \tau_N^{11} \\ \tau_N^{21} \\ \sigma_N^{21} \end{bmatrix} = x_-\Lambda_-J_R^{-1}$$

results in a strongly stable numerical scheme.

Proof Inserting the penalty parameters $[\tau_N^T,\ \tilde{\sigma}_N^T]^T = x_-\Lambda_-\bar{J}_R^{-1}$ into (6.7), yields

$$\begin{aligned} BT_R^D = &-\left(x_+^T\bar{V}_N - \mathscr{C}_R^{-1}R_R^*\Lambda_-\tilde{g}_R\right)^*\mathscr{C}_R\left(x_+^T\bar{V}_N - \mathscr{C}_R^{-1}R_R^*\Lambda_-\tilde{g}_R\right) \\ &-\tilde{g}_R^*\left(\Lambda_- - \Lambda_-R_R\mathscr{C}_R^{-1}R_R^*\Lambda_-\right)\tilde{g}_R + (\bar{L}_R\bar{V}_N - \hat{g}_R)^*J_R^{-*}\Lambda_-J_R^{-1}(\bar{L}_R\bar{V}_N - \hat{g}_R) \end{aligned} \tag{6.9}$$

where $\mathscr{C}_R \geq 0$ according to Proposition 6.2. □

Remark 6.2 Note that when using the penalty parameters as specified in Proposition 6.3 and 6.4, the discrete boundary terms $BT_{L,R}^D$ in (6.8) *and* (6.9) *correspond exactly to the continuous boundary terms $BT_{L,R}$ in* (6.4)*, except for a small damping term. The damping term is a function of the deviation from the boundary data, and goes to zero as the mesh is refined.*

7 Minor numerical details

As an example, we consider imposing the Dirichlet boundary conditions at the left boundary, and using the exact NRBC at the right boundary. Hence the term $(\Sigma_0 * V)(t) = \mathscr{L}^{-1}\{\hat{\Sigma}_0(s)\hat{V}(s)\}$ in (5.1) will be replaced by

$$(P^{-1}e_0 \otimes \tau_0^{Dir.} + P^{-1}D^Te_0 \otimes \sigma_0^{Dir.})(L_LV_0 - g_L). \tag{7.1}$$

Giving Dirichlet boundary conditions such that $U = g_L$ at the left boundary, implies that $L_L = I_2$. The penalty matrices in (7.1) are given in [10].

7.1 The convolution

At the right boundary we impose the non-reflecting boundary conditions. We follow the work in [33,34], and approximate the convolution $(\Sigma_N * V)(t) = \mathscr{L}^{-1}\{\hat{\Sigma}_N(s)\hat{V}(s)\}$ in (5.1) at time $t_n = nh$ by the convolution quadrature

$$(\Sigma_N * V)(t_n) = \int_0^{t_n}\Sigma_N(\tau)V(t_n - \tau)d\tau \approx \sum_{j=0}^{n}\omega_j(h)V(t_{n-j}), \tag{7.2}$$

where h is the time step, and where $\omega_j(h) \approx h\Sigma_N(t_j)$ for jh away from zero. The coefficients $\omega_j(h)$ in (7.2) are approximated by

$$\hat{\omega}_j(h) = \rho^{-j}\frac{1}{L}\sum_{l=0}^{L-1}\hat{\Sigma}_N\left(\frac{\delta(\rho e^{i\tau_l})}{h}\right)e^{-ij\tau_l}, \qquad \tau_l = 2\pi l/L. \tag{7.3}$$

The constants ρ and L and the function δ must be suitably chosen. We use $\rho = 0.975$, $L = T/h$, where T is the end time of the computation, and $\delta(\zeta) = \sum_{i=1}^{3}\frac{1}{i}(1-\zeta)^i$. These values of ρ, L and δ gave good results in our simulations but are not an optimized choice. However, the numerical convolution is not the main point of this paper and this choice suffices for our purpose. See [34] for more details on how these parameters affects the accuracy. Note that there exist more elaborate versions of this method, see e.g. [35] and [41], which are faster and less memory consuming. These and other approaches for approximating the convolution are discussed in [2].

7.2 The time discretization

We let the boundary data $\hat{g}_R$ be zero such that $\hat{\Gamma}_N = 0$ in (5.3) and $\Gamma_N = 0$ in (5.1). The semi-discrete scheme (5.1) is expressed as

$$V_t = \mathbf{F}(t,V) = \mathbf{A}V + \mathbf{G}(t) + \int_0^t \Sigma_N(\tau)V(t-\tau)d\tau, \tag{7.4}$$

where, including the Dirichlet boundary condition in (7.1),

$$\begin{aligned}\mathbf{A} &= -(D\otimes A) + (D^2\otimes B) + (P^{-1}e_0\otimes\tau_0^{Dir.} + P^{-1}D^Te_0\otimes\sigma_0^{Dir.})(e_0^T\otimes L_L)\\ \mathbf{G}(t) &= F - (P^{-1}e_0\otimes\tau_0^{Dir.} + P^{-1}D^Te_0\otimes\sigma_0^{Dir.})g_L(t).\end{aligned}$$

Equation (7.4) is discretized in time using the trapezoidal rule,

$$V_{n+1} = V_n + \frac{h}{2}\left(\mathbf{F}(t_n,V_n) + \mathbf{F}(t_{n+1},V_{n+1})\right). \tag{7.5}$$

We insert (7.4) into (7.5), and use the approximation

$$\int_0^t \Sigma_N(\tau)V(t-\tau)d\tau \approx \sum_{j=0}^{n}\hat{\omega}_j(h)V(t_{n-j}).$$

After moving all terms containing V_{n+1} to the left-hand side, we obtain the scheme

$$\begin{aligned}\left(I - \frac{h}{2}(\mathbf{A}+\hat{\omega}_0)\right)V_{n+1} = \left(I+\frac{h}{2}\mathbf{A}\right)V_n + \frac{h}{2}\sum_{j=0}^{n}\left(\hat{\omega}_j+\hat{\omega}_{j+1}\right)V_{n-j}\\ + \frac{h}{2}\left(\mathbf{G}(t_n)+\mathbf{G}(t_{n+1})\right).\end{aligned} \tag{7.6}$$

When computing $\hat{\omega}_j$ in (7.6), using (7.3), we need $\hat{\Sigma}_N$. We rewrite the parts of $\hat{\Sigma}_N\hat{V}$ in (5.6) such that we can identify

$$\hat{\Sigma}_N = \bar{P}^{-1}(E_N\otimes\tau_N H_R + D^TE_N\otimes\sigma_N H_R + E_ND\otimes\tau_N G_R + D^TE_ND\otimes\sigma_N G_R), \tag{7.7}$$

where $E_N = e_N e_N^T$. That is, $\hat{\Sigma}_N$ is a $2(N+1) \times 2(N+1)$ matrix, and consequently so are $\hat{\omega}_j$. Fortunately $\hat{\Sigma}_N$ is sparse since E_N mainly consist of zeroes, and it suffices to compute the lower right corner of $\hat{\omega}_j$.

Remark 7.1 The scheme (7.6) *exemplifies the special case when having the Dirichlet boundary conditions at the left boundary and the exact NRBC at the right boundary. Other scenarios, for example when having the exact NRBC's at the left boundary and the Dirichlet boundary condition at the right boundary, are derived in a similar way.*

7.3 The penalty parameters for the NRBC's

When computing $\hat{\Sigma}_N$ in (7.7), we need the penalty parameters τ_N and σ_N. First, the rotation $\widetilde{A} = X\Lambda X^T$ can be chosen in numerous ways, and the choice of rotation will influence the penalty parameters slightly. (To compute the eigenvalues and eigenvectors numerically is one option.) We have used the rotation

$$\Lambda_+ = \begin{bmatrix} \frac{1}{2(v+c)} & \\ & \frac{-v}{v^2-c^2} \end{bmatrix}, \quad \Lambda_- = \begin{bmatrix} \frac{1}{2(v-c)} \end{bmatrix}, \quad x_+ = \begin{bmatrix} v+c & 0 \\ v+c & 0 \\ -\varepsilon & \varepsilon \end{bmatrix}, \quad x_- = \begin{bmatrix} v-c \\ c-v \\ \varepsilon \end{bmatrix},$$

where $\Lambda = diag(\Lambda_+, \Lambda_-)$ and $X = [x_+, x_-]$, which yields

$$X^{-T} = \begin{bmatrix} \frac{1}{2(v+c)} & \frac{-c}{v^2-c^2} & \frac{1}{2(v-c)} \\ \frac{1}{2(v+c)} & \frac{v}{v^2-c^2} & \frac{-1}{2(v-c)} \\ 0 & \frac{1}{\varepsilon} & 0 \end{bmatrix}$$

and is valid for $0 < v < c$. Next, we rewrite $\bar{L}_R$ in (6.3) as $\bar{L}_R = [J_R R_R \; J_R] X^T$. The matrix J_R is then obtained from $\bar{L}_R X^{-T}$, where $\bar{L}_R$ are given in (3.8), as

$$\bar{L}_R X^{-T} = \begin{bmatrix} \frac{\alpha_3+\beta_3}{2(v+c)} & \frac{v\beta_3 - c\alpha_3}{v^2-c^2} + 1 & \underbrace{\frac{\alpha_3-\beta_3}{2(v-c)}}_{J_R} \end{bmatrix}.$$

Thereafter the penalty parameters are computed as specified in Proposition 6.3 and Proposition 6.4, such that we obtain

$$\tau_N = \begin{bmatrix} v-c \\ c-v \end{bmatrix} \Lambda_- J_R^{-1}, \qquad \sigma_N = \begin{bmatrix} 0 \\ \varepsilon \end{bmatrix} \Lambda_- J_R^{-1}. \tag{7.8}$$

Remark 7.2 In the numerical experiments we will compare the exact NRBC's to a low order approximation of the NRBC's. The approximative NRBC's are derived by inserting $s = 0$ into the exact non-reflecting boundary operators, which yields time-local, low-reflecting boundary conditions. The penalty parameters are obtained similarly, by inserting $s = 0$ into $\tau_{0,N}$ and $\sigma_{0,N}$. The resulting operators are given in [10].

7.4 The penalty parameters in the hyperbolic limit

In the numerical scheme the boundary operators (3.10) are multiplied by the penalty parameters $\tau_{0,N}$ and $\sigma_{0,N}$. With the rotation of our choice, given in Section 7.3, we will for $\varepsilon = 0$ (and $0 < v < c$) have

$$J_L = \begin{bmatrix} 0 & 1 \\ -1 & 0 \end{bmatrix}, \qquad J_R = 1,$$

which yields

$$\tau_0 = \begin{bmatrix} 0 & 1/2 \\ 0 & 1/2 \end{bmatrix} \qquad \sigma_0 = \begin{bmatrix} 0 & 0 \\ 0 & 0 \end{bmatrix} \qquad \tau_N = \begin{bmatrix} 1/2 \\ -1/2 \end{bmatrix} \qquad \sigma_N = \begin{bmatrix} 0 \\ 0 \end{bmatrix}.$$

This shows that the method behaves well also in the $\varepsilon \to 0$ limit.

8 Numerical results

We let the computational domain be $[x_L, x_R] = [0, 1]$, and as reference solution we use the solution from a five times larger domain. The errors are defined as the difference between the solution and the reference solution, as $\Delta p = p - p^{ref}$ and $\Delta u = u - u^{ref}$. The SBP matrix P is used for computing norms of the errors, as $\text{Error}(p) = \|\Delta p\|_P$ and $\text{Error}(u) = \|\Delta u\|_P$, where the norm of a vector $\mathbf{v}$ is defined as $\|\mathbf{v}\|_P^2 = \mathbf{v}^T P \mathbf{v}$. See [26] for details on the accuracy and interpretations of SBP norms. For the space discretization we use a third order accurate SBP scheme, and as mentioned earlier, the trapezoidal rule is used for the time discretization. In all simulations, if not stated otherwise, we use the physical parameter values $c = 1$, $v = 0.5$ and $\varepsilon = 0.1$. The time step is $h = 0.001$ and the end time $T = 0.4$. The number of grid point varies, but in the figures we have used $N = 64$. The time step is sufficiently small, such that the errors from the space discretization are dominating. To reduce the number of figures we only show the solution for the variable u, but the results for the variable p are similar and presented in the tables.

8.1 Non-reflecting boundary conditions at the right boundary

First, simulations are performed using the scheme (7.6) with the penalty parameters given in (7.8). As initial condition we use

$$p(x,0) = u(x,0) = \begin{cases} 0 & 0.05 \geq x \\ cos^3(2.5\pi(x-0.25)) & 0.05 < x < 0.45 \\ 0 & 0.45 \leq x. \end{cases} \tag{8.1}$$

At the left boundary the Dirichlet boundary conditions are imposed and at the right boundary the solution is supposed to propagate out without reflections. This is the same problem setup as in the introducing examples in Figure 1.1 and Table 1.1. In comparison the exact NRBC outperforms those examples by far, see Figure 8.1. More importantly, the exact NRBC solution converges to the reference solution as the mesh

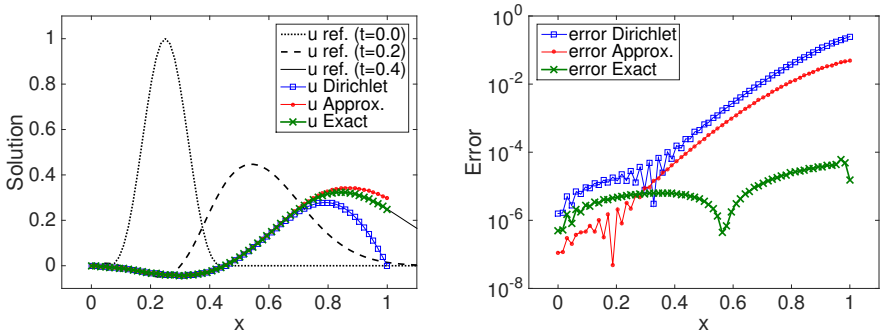

(a) Solution at $t = 0.4$ (b) Error at $t = 0.4$

Fig. 8.1 The solution to (2.1) with initial condition given by (8.1). At the right boundary the Dirichlet boundary condition, the approximate NRBC or the exact NRBC is used.

is refined, see Table 8.1. It might be expected that the error should be almost at machine precision for the exact boundary conditions. However, the boundary conditions derived here are exact for the continuous problem – not for the discrete one – and still have to be approximated using a numerical scheme. For the reference solution the boundary closure is at $x = 5$ instead of at $x = 1$, which implies that the numerical stencils differ and consequently produce different solutions even with exact data.

Table 8.1 Results obtained using the exact NRBC at the right boundary.

N	Error(p)	ratio	conv. rate	Error(u)	ratio	conv. rate
16	0.00091109			0.00121302		
32	0.00010158	8.9690	3.1649	0.00014664	8.2722	3.0483
64	0.00001152	8.8217	3.1411	0.00001872	7.8317	2.9693
128	0.00000139	8.2978	3.0527	0.00000241	7.7753	2.9589

In the simulations done here, the computational cost when using the exact NRBC's are the same as when using any of the other boundary conditions. However, for longer simulation times it would probably be better to use a more advanced version of the method, as already discussed in Section 7.1.

8.2 Non-reflecting boundary conditions at the left boundary

Next we consider the NRBC's at the left boundary (and impose Dirichlet boundary conditions at the right boundary). For this case we use the initial condition

$$p(x,0) = -u(x,0) = \begin{cases} 0 & 0.3 \geq x \\ -cos^3(2.5\pi(x-0.5)) & 0.3 < x < 0.7 \\ 0 & 0.7 \leq x, \end{cases} \tag{8.2}$$

such that the main content of the initial solution travels in the left direction. The resulting solution at time $t = 0.4$ is shown in Figure 8.2, and as can be seen in Table 8.2 the solution converges to the reference solution as the mesh is refined.

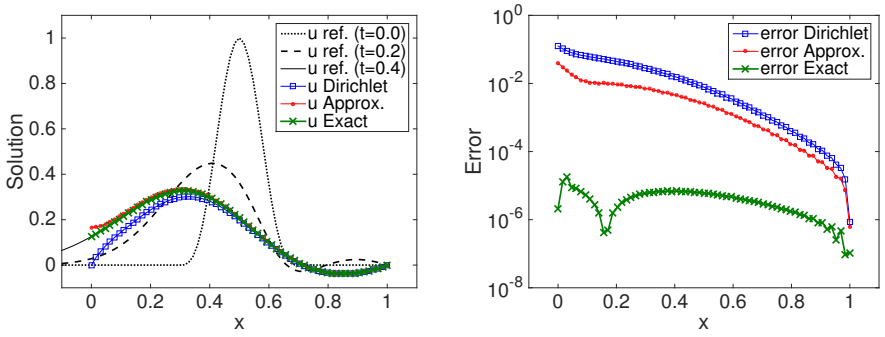

(a) Solution at $t = 0.4$ (b) Error at $t = 0.4$

Fig. 8.2 The solution to (2.1) with initial condition given by (8.2). At the left boundary the Dirichlet boundary condition, the approximate NRBC or the exact NRBC is imposed.

Table 8.2 Results obtained using the exact NRBC at the left boundary.

N	Error(p)	ratio	conv. rate	Error(u)	ratio	conv. rate
16	0.00026816			0.00036867		
32	0.00003824	7.0134	2.8101	0.00005167	7.1355	2.8350
64	0.00000414	9.2323	3.2067	0.00000522	9.9028	3.3078
128	0.00000051	8.0689	3.0124	0.00000064	8.1321	3.0236

8.3 Initial condition without compact support

In the boundary conditions (3.7) the possibility of perturbed data, due to an unknown particular solution, is indicated. To investigate what impact that lack of knowledge has on the result we consider an initial condition that does not have compact support in $x \in [0,1]$,

$$p(x,0) = u(x,0) = \begin{cases} 0 & 0.7 \geq x \\ cos^3(2.5\pi(x-0.9)) & 0.7 < x < 1.1 \\ 0 & 1.1 \leq x, \end{cases} \tag{8.3}$$

where $p(1,0) = u(1,0) \approx 0.35$. We thus know that g'_R in (3.7) is non-zero for this problem. Even so, we again impose zero boundary data to the non-reflecting boundary condition with the purpose of testing the robustness of the method. The results for the exact NRBC's are still superior compared to the ones obtained with the Dirichlet or the approximate NRBC's, see Figure 8.3. This example shows that the exact NRBC's derived perform well even under non-optimal conditions.

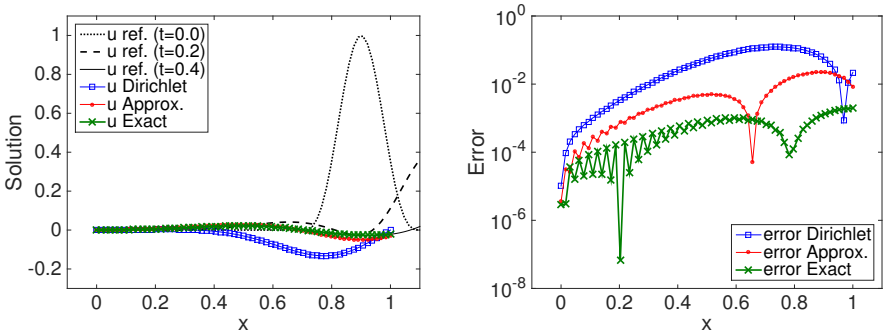

(a) Solution at $t = 0.4$ (b) Error at $t = 0.4$

Fig. 8.3 The solution to (2.1) with initial condition given by (8.3) (initial condition without compact support). At the right boundary the Dirichlet boundary condition, the approximate NRBC or the exact NRBC is imposed.

8.4 Numerical results in the hyperbolic limit

We test the behaviour of the boundary conditions in the hyperbolic limit by varying ε, while keeping the other parameters identical to those in Sect 8.1. The result for $\varepsilon = 0.01$ is shown in Figure 8.4.

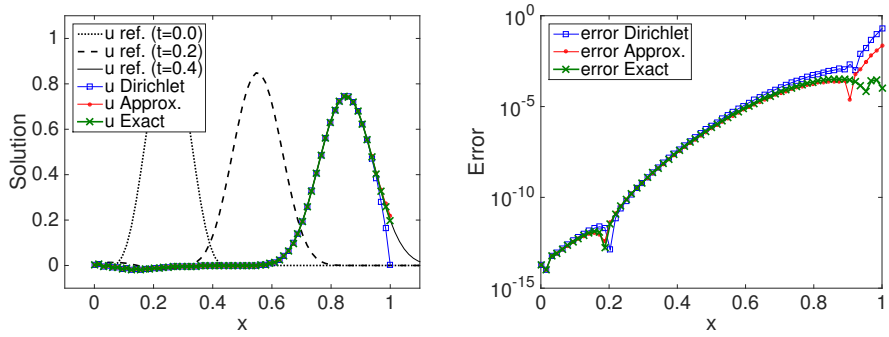

(a) Solution at $t = 0.4$, $\varepsilon = 0.01$ (b) Error at $t = 0.4$, $\varepsilon = 0.01$

Fig. 8.4 The solution to (2.1) with initial condition given by (8.1), now with $\varepsilon = 0.01$ instead of the earlier $\varepsilon = 0.1$. At the right boundary the Dirichlet boundary condition, the approximate NRBC or the exact NRBC is used.

As ε decreases, the solution converges to the hyperbolic solution, see Figure 8.5. This holds also for the approximative NRBC's (which are in fact exact for $\varepsilon = 0$). The fact that the boundary conditions transition smoothly to the hyperbolic ones without need of modifying the numerical boundary procedure is an advantageous property of the SAT technique, see [45, 1, 8].

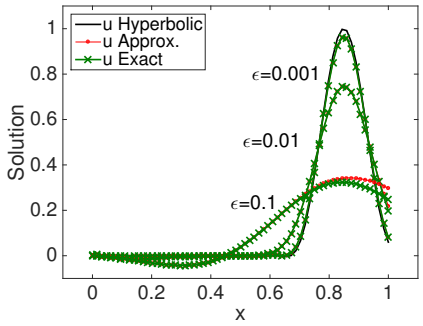

(a) Solution at $t = 0.4$

Fig. 8.5 At the right boundary the approximate NRBC or the exact NRBC is used. The incompletely parabolic solutions converge to the hyperbolic solution as $\varepsilon \to 0$.

9 Summary and conclusions

We have investigated exact non-reflecting boundary conditions (NRBC) with focus on the theoretical aspects, well-posedness and stability. We considered an incompletely parabolic system of partial differential equations, as a model of the compressible Navier-Stokes equations. The exact NRBC's were derived in Laplace transformed space.

We expressed the transformed solution as a superposition of ingoing and outgoing waves, and eliminated the ingoing waves at each boundary. Both inflow and outflow NRBC's were derived. It was shown that the exact non-reflecting boundary conditions lead to well-posedness, both in the sense of Kreiss and in the energy sense.

The system was discretized in space using a high order accurate finite difference scheme on summation by parts form (SBP), and the boundary conditions were imposed weakly using a penalty formulation (SAT). With the continuous energy estimate as a guideline, a SAT formulation was derived, which led to a discrete energy estimate very similar to the continuous one. Hence, by the combined use of the SBP operators and the SAT implementation, stability followed directly from the result of well-posedness for the continuous problem.

Both the fact that non-reflecting boundary conditions lead to well-posedness, and that this automatically leads to stability using the SBP-SAT technique, are new results.

We have compared the exact NRBC's to the Dirichlet boundary conditions and to approximate NRBC's. The exact NRBC's outperformed the other conditions, and led to lower reflections both for exact and erroneous boundary data. In contrast to the approximative non-reflecting boundary conditions and the Dirichlet boundary conditions, convergence to the correct solution was obtained for the exact conditions when the mesh was refined (and exact boundary data was available). With decreased viscosity both the exact and the approximative NRBC's converge smoothly to the characteristic boundary conditions of the purely hyperbolic problem, without any need of changes in the numerical procedure.

The superior accuracy, both on the boundary and in the interior (owing to the exact NRBC's and the high order scheme, respectively), in combination with the guaranteed stability, resulted in a competitive numerical method for computations on unbounded domains.

A Multiple roots

We show that the polynomial $q(\kappa,s)$ in (2.4) has no multiple roots κ for $\mathrm{Re}(s)\geq 0$, unless $s=0$. We start by writing $\tilde{q}(\kappa,s)=-q(\kappa,s)/(\varepsilon v)$ as

$$\tilde{q}(\kappa,s)=\kappa^3-r_2\kappa^2+r_1\kappa-r_0$$

where the coefficients r_0, r_1 and r_2 are given in (3.2). The derivative $\tilde{q}'(\kappa,s)=\frac{\partial}{\partial\kappa}\tilde{q}(\kappa,s)=3\kappa^2-2r_2\kappa+r_1$ has roots $\kappa_{4,5}=r_2/3\pm\sqrt{((r_2/3)^2-r_1/3}$. If the polynomial $\tilde{q}(\kappa,s)$ has a multiple root κ_j, then that root κ_j will be a solution to the derivative $\tilde{q}'(\kappa,s)$ as well. To check whether $\tilde{q}(\kappa,s)$ and $\tilde{q}'(\kappa,s)$ have any roots in common, we insert $\kappa_{4,5}$ into $\tilde{q}(\kappa,s)$. This yields

$$\tilde{q}(\kappa_{4,5},s)=\frac{-1}{27}\left(r_2\left(2r_2^2-9r_1\right)\pm 2\sqrt{r_2^2-3r_1}\left(r_2^2-3r_1\right)+27r_0\right).$$

Requiring $\tilde{q}(\kappa_{4,5},s)=0$ leads to $r_2\left(2r_2^2-9r_1\right)+27r_0=\mp 2\sqrt{r_2^2-3r_1}\left(r_2^2-3r_1\right)$, which we square on both sides to obtain

$$\left(r_2\left(2r_2^2-9r_1\right)+27r_0\right)^2=4\left(r_2^2-3r_1\right)^3. \tag{A.1}$$

If the relation (A.1) is fulfilled $q(\kappa,s)$ has a multiple root. We check if this can occur by defining $\Upsilon=\left(r_2\left(2r_2^2-9r_1\right)+27r_0\right)^2-4\left(r_2^2-3r_1\right)^3$, and see whether it is possible to find $\Upsilon=0$. Inserting the values $r_0=s^2/(\varepsilon v)$, $r_1=-2s/\varepsilon$ and $r_2=(v^2-c^2-s\varepsilon)/(\varepsilon v)$ from (3.2) gives

$$\Upsilon=-27\frac{s^2}{\varepsilon^4v^4}\left(4c^2(v^2-c^2)^2+4c^2(3c^2+5v^2)s\varepsilon+(v^2+12c^2)(s\varepsilon)^2+4(s\varepsilon)^3\right).$$

Let $s\varepsilon=\tilde{\eta}+\tilde{\xi}i$ to split Υ into one real and one imaginary part, as

$$\begin{aligned}\Upsilon=&-27\frac{s^2}{\varepsilon^4v^4}\left(4c^2(v^2-c^2)^2+4c^2(3c^2+5v^2)\tilde{\eta}+(v^2+12c^2)(\tilde{\eta}^2-\tilde{\xi}^2)+4(\tilde{\eta}^3-3\tilde{\eta}\tilde{\xi}^2)\right)\\&-27\frac{s^2}{\varepsilon^4v^4}\left(4c^2(3c^2+5v^2)+2(v^2+12c^2)\tilde{\eta}+4(3\tilde{\eta}^2-\tilde{\xi}^2)\right)\tilde{\xi}i.\end{aligned}$$

The imaginary part of Υ can be cancelled either by choosing $\tilde{\xi}=0$ or by choosing $\tilde{\xi}^2=c^2(3c^2+5v^2)+(v^2+12c^2)\tilde{\eta}/2+3\tilde{\eta}^2$. In both these cases the real part of Υ can only be cancelled if $\tilde{\eta}<0$. The only exception is if $s=0$, then a multiple root is possible. This case is considered next.

A.1 Multiple roots in the $s=0$ case

For $s=0$ the polynomial in (2.4) becomes $q(\kappa,0)=(v^2-c^2)\kappa^2-\varepsilon v\kappa^3$, and has roots

$$\begin{aligned}0<v<c:&\quad \kappa_1=\frac{v^2-c^2}{\varepsilon v},&\quad \kappa_2=0,&\quad \kappa_3=0\\ v=c:&\quad \kappa_1=0,&\quad \kappa_2=0,&\quad \kappa_3=0\\ v>c:&\quad \kappa_1=0,&\quad \kappa_2=0,&\quad \kappa_3=\frac{v^2-c^2}{\varepsilon v}.\end{aligned}$$

If $v \neq c$, we can find two linearly independent eigenvectors corresponding to the double root $\kappa = 0$, so in that case the single root ansatz $\bar{U}_h = e^{\kappa x}\Psi$ still holds. When $v = c$, $\kappa = 0$ is a triple root, but we can only find two linearly independent eigenvectors and hence the single root ansatz is no longer valid.

This can also be seen from the $s \to 0$ limit of $\Phi_i^T\Psi_i$ (the diagonal entries of $E(s)$ in Proposition 4.1). Under the assumption $|s| << 1$ the approximate values of κ_j and $\Phi_i^T\Psi_i$ can be computed. For $0 < v < c$ we get

$$\kappa_1 = \frac{v^2-c^2}{\varepsilon v} + \mathscr{O}(s), \qquad \kappa_2 = \frac{-s}{v+c} + \mathscr{O}(s^2), \qquad \kappa_3 = \frac{-s}{v-c} + \mathscr{O}(s^2)$$
$$\Phi_1^T\Psi_1 = v^2 - c^2 + \mathscr{O}(s), \qquad \Phi_2^T\Psi_2 = 2c(v+c) + \mathscr{O}(s), \qquad \Phi_3^T\Psi_3 = -2c(v-c) + \mathscr{O}(s),$$

and for $v > c$ we have the same relations, except that the expression for κ_1 has become κ_3, and vice versa. In both these cases we see that $\Phi_i^T\Psi_i \neq 0$ and hence $E(0)$ is non-singular. However, the above approximations only hold for $v \neq c$. For $v = c$ the κ_j's and $\Phi_i^T\Psi_i$'s are

$$\kappa_1 = -\sqrt{\frac{2s}{\varepsilon}} + \mathscr{O}(s), \qquad \kappa_2 = \frac{-s}{2c} + \mathscr{O}(s^2), \qquad \kappa_3 = \sqrt{\frac{2s}{\varepsilon}} + \mathscr{O}(s)$$
$$\Phi_1^T\Psi_1 = -2c\sqrt{2s\varepsilon} + \mathscr{O}(s), \qquad \Phi_2^T\Psi_2 = 4c^2 + \mathscr{O}(s), \qquad \Phi_3^T\Psi_3 = 2c\sqrt{2s\varepsilon} + \mathscr{O}(s).$$

We see that both $\Phi_1^T\Psi_1$ and $\Phi_3^T\Psi_3$ become zero for $s = 0$, and consequently the matrix $E(s)$ in Proposition 4.1 is in fact singular for $s = 0$ and $v = c$. In this case the ansatz $\bar{U}_h = e^{\kappa x}\Psi$ and the general homogeneous solution (2.5) must be replaced by a double root ansatz. In this paper we will simply avoid the special case $v \neq c$.

B The signs of $\mathrm{Re}(\kappa/s)$

Consider the roots κ_j of the polynomial $q(\kappa, s)$ in (2.4). We show that $\mathrm{Re}(\kappa_j/s)$ has the same sign as $\mathrm{Re}(\kappa_j)$ for $j = 1,2,3$. Start by denoting $\tilde{\kappa} = \kappa/s$, such that $q(\kappa, s)$ becomes

$$q(s\tilde{\kappa}, s) = s^2\left(1 + 2v\tilde{\kappa} + (v^2 - c^2 - \varepsilon s)\tilde{\kappa}^2 - s\varepsilon v\tilde{\kappa}^3\right) = 0.$$

Let $s = \eta + \xi i$ and assume that $\tilde{\kappa}$ passes the imaginary axis, i.e. $\tilde{\kappa} = \tilde{\beta} i$. Inserting this into $q(s\tilde{\kappa}, s)$ and dividing by s^2 (assuming $s \neq 0$) yields

$$1 - (v^2 - c^2 - \varepsilon\eta + v\varepsilon\xi\tilde{\beta})\tilde{\beta}^2 + (2v + \varepsilon\xi\tilde{\beta} + v\varepsilon\eta\tilde{\beta}^2)\tilde{\beta} i = 0. \tag{B.1}$$

There are two options that make the imaginary part of (B.1) zero. Either we let $\tilde{\beta} = 0$ or we let $2v + \varepsilon\xi\tilde{\beta} + v\varepsilon\eta\tilde{\beta}^2 = 0$. For $\eta \geq 0$, both these choices results in a non-zero real part of (B.1). We know already that the signs of $\mathrm{Re}(\kappa_j/s)$ are equal to the signs of $\mathrm{Re}(\kappa_j)$ when s is real and positive, and thus $\mathrm{Re}(\kappa_1/s) < 0$, $\mathrm{Re}(\kappa_2/s) < 0$ and $\mathrm{Re}(\kappa_3/s) > 0$ for all $\mathrm{Re}(s) > 0$.

C Proofs of Proposition 4.2 and Proposition 4.3

When computing $\mathscr{A}_L$ and $\mathscr{A}_R$ in (4.4) and (4.5) we need $\Psi_j^* \widetilde{A}\Psi_i$, where $\widetilde{A}$ and Ψ_i are given in (4.3) and (3.3), respectively. First, we compute

$$\widetilde{A}\Psi_i = \begin{bmatrix} v & c & 0 \\ c & v & -\varepsilon \\ 0 & -\varepsilon & 0 \end{bmatrix} \begin{bmatrix} -c \\ (s + v\kappa_i)/\kappa_i \\ s + v\kappa_i \end{bmatrix} = \begin{bmatrix} -vc + c(s + v\kappa_i)/\kappa_i \\ -c^2 + v(s + v\kappa_i)/\kappa_i - \varepsilon(s + v\kappa_i) \\ -\varepsilon(s + v\kappa_i)/\kappa_i \end{bmatrix}$$
$$= \begin{bmatrix} cs/\kappa_i \\ ((v^2 - c^2 - \varepsilon s)\kappa_i^2 - \varepsilon v\kappa_i^3)/\kappa_i^2 + vs/\kappa_i \\ -\varepsilon(s + v\kappa_i)/\kappa_i \end{bmatrix} = \begin{bmatrix} cs/\kappa_i \\ -s(s + v\kappa_i)/\kappa_i^2 \\ -\varepsilon(s + v\kappa_i)/\kappa_i \end{bmatrix}.$$

In the last step we have used that $(v^2-c^2-s\varepsilon)\kappa^2-\varepsilon v\kappa^3=-(s^2+2sv\kappa)$ from (2.4). Next we compute

$$\begin{aligned}\Psi_j^*\widetilde{A}\Psi_i &= \begin{bmatrix} -c \\ (s+v\kappa_j)/\kappa_j \\ s+v\kappa_j \end{bmatrix}^* \begin{bmatrix} cs/\kappa_i \\ -s(s+v\kappa_i)/\kappa_i^2 \\ -\varepsilon(s+v\kappa_i)/\kappa_i \end{bmatrix} \\ &= -\frac{s}{\kappa_i}\left(c^2+\left(\frac{s+v\kappa_j}{\kappa_j}\right)^*\left(\frac{s+v\kappa_i}{\kappa_i}\right)\right)-\frac{\varepsilon}{\kappa_i}(s+v\kappa_j)^*(s+v\kappa_i), \end{aligned} \tag{C.1}$$

and since $\widetilde{A}$ is symmetric it is also possible to compute $\Psi_j^*\widetilde{A}\Psi_i$ as

$$\Psi_j^*\widetilde{A}\Psi_i=(\widetilde{A}\Psi_j)^*\Psi_i=-\frac{s^*}{\kappa_j^*}\left(c^2+\left(\frac{s+v\kappa_j}{\kappa_j}\right)^*\left(\frac{s+v\kappa_i}{\kappa_i}\right)\right)-\frac{\varepsilon}{\kappa_j^*}(s+v\kappa_j)^*(s+v\kappa_i). \tag{C.2}$$

By simply taking the average of (C.1) and (C.2) we obtain

$$\Psi_j^*\widetilde{A}\Psi_i=-\frac{1}{2}\left(\frac{s}{\kappa_i}+\frac{s^*}{\kappa_j^*}\right)\left(c^2+\left(\frac{s+v\kappa_j}{\kappa_j}\right)^*\left(\frac{s+v\kappa_i}{\kappa_i}\right)\right)-\frac{\varepsilon}{2}\left(\kappa_i+\kappa_j^*\right)\left(\frac{s+v\kappa_j}{\kappa_j}\right)^*\left(\frac{s+v\kappa_i}{\kappa_i}\right). \tag{C.3}$$

Inserting $i=j=3$ into (C.3) yields $\mathscr{A}_L=\Psi_3^*\widetilde{A}\Psi_3$ and the result stated in (4.4).

C.1 Proof of Proposition 4.3

Proof The right boundary condition in (3.5) yields the solution $\bar{U}_h=\sigma_1 e^{\kappa_1 x}\Psi_1+\sigma_2 e^{\kappa_2 x}\Psi_2$. Inserting this into BT_R in (4.3) we obtain

$$BT_R=-\begin{bmatrix}\sigma_1 e^{\kappa_1 x_R}\\ \sigma_2 e^{\kappa_2 x_R}\end{bmatrix}^*\mathscr{A}_R\begin{bmatrix}\sigma_1 e^{\kappa_1 x_R}\\ \sigma_2 e^{\kappa_2 x_R}\end{bmatrix},\qquad\qquad \mathscr{A}_R=\begin{bmatrix}\Psi_1^*\widetilde{A}\Psi_1 & \Psi_1^*\widetilde{A}\Psi_2\\ \Psi_2^*\widetilde{A}\Psi_1 & \Psi_2^*\widetilde{A}\Psi_2\end{bmatrix},$$

where $\mathscr{A}_R$ is a Hermitian matrix. To show that $\mathscr{A}_R\geq 0$ we first note that the diagonal elements of $\mathscr{A}_R$, $\Psi_1^*\widetilde{A}\Psi_1$ and $\Psi_2^*\widetilde{A}\Psi_2$, are both positive for $\mathrm{Re}(s)>0$. This can be seen by inserting $j=i$ into (C.3) as

$$\Psi_i^*\widetilde{A}\Psi_i=-\mathrm{Re}\left(\frac{s}{\kappa_i}\right)\left(c^2+\left|\frac{s+v\kappa_i}{\kappa_i}\right|^2\right)-\varepsilon\mathrm{Re}\left(\kappa_i\right)\left|\frac{s+v\kappa_i}{\kappa_i}\right|^2\geq 0,\qquad\qquad \text{for } i=1,2,$$

where we have used that $\mathrm{Re}(\kappa_i/s)<0$ and $\mathrm{Re}(\kappa_i)<0$ for $i=1,2$. Moreover, the off-diagonal elements $\Psi_j^*\widetilde{A}\Psi_i$ must be sufficiently small, which they are if the quantity $\gamma=(\Psi_1^*\widetilde{A}\Psi_1)(\Psi_2^*\widetilde{A}\Psi_2)-(\Psi_1^*\widetilde{A}\Psi_2)(\Psi_2^*\widetilde{A}\Psi_1)$ is positive. By using (C.1) or (C.2) (followed by the argument that γ is real) it is possible to write

$$\gamma=\left(\mathrm{Re}\left(\frac{s\varepsilon}{\kappa_1\kappa_2}\right)\left(c^2v^2+\left|\frac{s+v\kappa_1}{\kappa_1}\right|^2\left|\frac{s+v\kappa_2}{\kappa_2}\right|^2\right)+\mathrm{Re}\left(\frac{s^2}{\kappa_1\kappa_2}\right)\frac{c^2|s|^2}{|\kappa_1\kappa_2|^2}\right)|\kappa_1-\kappa_2|^2$$

where the terms $s\varepsilon/(\kappa_1\kappa_2)$ and $s^2/(\kappa_1\kappa_2)$ have positive real parts. This is realized by using the relation $\kappa_1\kappa_2\kappa_3=s^2/(\varepsilon v)$ in (3.2), which leads to

$$\frac{s\varepsilon}{\kappa_1\kappa_2}=\varepsilon^2 v\frac{\kappa_3}{s},\qquad\qquad \frac{s^2}{\kappa_1\kappa_2}=\varepsilon v\kappa_3$$

where $\mathrm{Re}(\kappa_3/s)\geq 0$ and $\mathrm{Re}(\kappa_3)\geq 0$ according to Proposition 3.1 and Proposition 3.2. Hence $\gamma\geq 0$ and consequently $\mathscr{A}_R$ is positive definite and $BT_R\leq 0$.

□

References

1. Abbas, Q., Nordström, J.: Weak versus strong no-slip boundary conditions for the Navier–Stokes equations. ENG APPL COMP FLUID **4**(1), 29–38 (2010)
2. Antoine, X., Arnold, A., Besse, C., Ehrhardt, M., Schädle, A.: A review of transparent and artificial boundary conditions techniques for linear and nonlinear Schrödinger equations. Commun. Comput. Phys. **4**(4), 729–796 (2008)
3. Appelö, D., Hagstrom, T.: A general perfectly matched layer model for hyperbolic-parabolic systems. SIAM J. Sci. Comput. **31**(5), 3301–3323 (2009)
4. Appelö, D., Hagstrom, T., Kreiss, G.: Perfectly matched layers for hyperbolic systems: General formulation, well-posedness, and stability. SIAM J. Appl. Math. **67**(1), 1–23 (2006)
5. Bécache, E., Givoli, D., Hagstrom, T.: High-order absorbing boundary conditions for anisotropic and convective wave equations. J. Comput. Phys. **229**(4), 1099–1129 (2010)
6. Berenger, J.: A perfectly matched layer for the absorption of electromagnetic waves. J. Comput. Phys. **114**(2), 185–200 (1994)
7. Carpenter, M.H., Gottlieb, D., Abarbanel, S.: Time-stable boundary conditions for finite-difference schemes solving hyperbolic systems: Methodology and application to high-order compact schemes. J. Comput. Phys. **111**(2), 220–236 (1994)
8. Efraimsson, G., Gong, J., Svärd, M., Nordström, J.: An investigation of the performance of a high-order accurate Navier–Stokes code. In: Proc. ECCOMAS CFD Conference 2006, pp. 11–. Tech. Univ. of Delft (2006)
9. Engquist, B., Majda, A.: Absorbing boundary conditions for the numerical simulation of waves. Math. Comput. **31**(139), 629–651 (1977)
10. Eriksson, S., Nordström, J.: Exact non-reflecting boundary conditions revisited : well-posedness and stability. Tech. Rep. 2012-032, Uppsala University, Division of Scientific Computing (2012)
11. Eskin, G.: Initial-boundary value problem for hyperbolic equations. In: Proceedings of the International Congress of Mathematicians. August 16-24, Warszawa (1983)
12. Ferm, L.: Non-reflecting boundary conditions for the steady Euler equations. J. Comput. Phys. **122**, 307–316 (1995)
13. Grote, M.J., Keller, J.B.: Nonreflecting boundary conditions for time-dependent scattering. J. Comput. Phys. **127**(1), 52–65 (1996)
14. Gustafsson, B.: Far-field boundary conditions for time-dependent hyperbolic systems. SIAM J. Sci. Statist. Comput. **9**(5), 812–828 (1988)
15. Gustafsson, B., Kreiss, H.O.: Boundary conditions for time dependent problems with an artificial boundary. J. Comput. Phys. **30**(3), 333–351 (1979)
16. Gustafsson, B., Kreiss, H.O., Oliger, J.: Time Dependent Problems and Difference Methods. John Wiley & Sons, Inc. (1995)
17. Gustafsson, B., Kreiss, H.O., Sundström, A.: Stability theory of difference approximations for mixed initial boundary value problems. II. Math. Comput. **26**(119), 649–686 (1972)
18. Hagstrom, T.: Asymptotic expansions and boundary conditions for time-dependent problems. SIAM J. Numer. Anal. **23**(5), 948–958 (1986)
19. Hagstrom, T.: Boundary conditions at outflow for a problem with transport and diffusion. J. Comput. Phys. **69**, 69–80 (1987)
20. Hagstrom, T.: Radiation boundary conditions for the numerical simulation of waves. Acta Numer. **8**, 47–106 (1999)
21. Hagstrom, T., Bécache, E., Givoli, D., Stein, K.: Complete radiation boundary conditions for convective waves. Commun. Comput. Phys. **11**(2), 610–628 (2012)
22. Hagstrom, T., Keller, H.B.: The numerical calculation of traveling wave solutions of nonlinear parabolic equations. SIAM J. Sci. Stat. Comput. **7**(3), 978–988 (1986)
23. Halpern, L.: Absorbing boundary conditions for the discretization schemes of the one-dimensional wave equation. Math. Comput. **38**(158), 415–429 (1982)
24. Halpern, L.: Artificial boundary conditions for incompletely parabolic perturbations of hyperbolic systems. SIAM J. Math. Anal. **22**(5), 1256–1283 (1991)
25. Hesthaven, J.: On the analysis and construction of perfectly matched layers for the linearized Euler equations. J. Comput. Phys. **142**(1), 129–147 (1998)
26. Hicken, J., Zingg, D.: Summation-by-parts operators and high-order quadrature. J. Comput. Appl. Math. **237**(1), 111–125 (2013)

27. Higdon, R.: Absorbing boundary conditions for difference approximations to the multi-dimensional wave equation. Math. Comput. **47**(176), 437–459 (1986)
28. Hu, F.Q., Li, X., Lin, D.: Absorbing boundary conditions for nonlinear Euler and Navier–Stokes equations based on the perfectly matched layer technique. J. Comput. Phys. **227**, 4398–4424 (2008)
29. Kopriva, D.A., Gassner, G.J.: An energy stable discontinuous Galerkin spectral element discretization for variable coefficient advection problems. SIAM J. Sci. Comput. **36**(4), 2076–2099 (2014)
30. Kreiss, H.O.: Initial boundary value problems for hyperbolic systems. Commun. Pure Appl. Math. **23**(3), 277–298 (1970)
31. Kreiss, H.O., Lorenz, J.: Initial-boundary value problems and the Navier–Stokes equations. Academic Press, New York (1989)
32. Lantos, N., Nataf, F.: Perfectly matched layers for the heat and advection-diffusion equations. J. Comput. Phys. **229**, 9042–9052 (2010)
33. Lubich, C.: Convolution quadrature and discretized operational calculus. I. Numer. Math **52**, 129–145 (1988)
34. Lubich, C.: Convolution quadrature and discretized operational calculus. II. Numer. Math **52**, 413–425 (1988)
35. Lubich, C., Schädle, A.: Fast convolution for nonreflecting boundary conditions. SIAM J. Sci. Comput. **24**(1), 161–182 (2002)
36. Nordström, J., Carpenter, M.H.: Boundary and interface conditions for high order finite difference methods applied to the Euler and Navier–Stokes equations. J. Comput. Phys. **148**, 621–645 (1999)
37. Nordström, J., Eriksson, S., Eliasson, P.: Weak and strong wall boundary procedures and convergence to steady-state of the Navier–Stokes equations. J. Comput. Phys. **231**(14), 4867–4884 (2012)
38. Nordström, J., Gong, J., van der Weide, E., Svärd, M.: A stable and conservative high order multi-block method for the compressible Navier–Stokes equations. J. Comput. Phys. **228**(24), 9020–9035 (2009)
39. Råde, L., Westergren, B.: Mathematics Handbook for Science and Engineering. Studentlitteratur, Lund (1998)
40. Rowley, C., Colonius, T.: Discretely nonreflecting boundary conditions for linear hyperbolic systems. J. Comput. Phys. **157**(2), 500–538 (2000)
41. Schädle, A., López-Fernández, M., Lubich, C.: Fast and oblivious convolution quadrature. SIAM J. Sci. Comp. **28**, 421–438 (2006)
42. Strand, B.: Summation by parts for finite difference approximation for d/dx. J. Comput. Phys. **110**(1), 47–67 (1994)
43. Strikwerda, J.C.: Initial boundary value problems for incompletely parabolic systems. Commun. Pure Appl. Math. **30**(6), 797–822 (1977)
44. Svärd, M., Carpenter, M., Nordström, J.: A stable high-order finite difference scheme for the compressible Navier–Stokes equations: Far-field boundary conditions. J. Comput. Phys. **225**(1), 1020–1038 (2007)
45. Svärd, M., Nordström, J.: A stable high-order finite difference scheme for the compressible Navier–Stokes equations: No-slip wall boundary conditions. J. Comput. Phys. **227**(10), 4805–4824 (2008)
46. Svärd, M., Nordström, J.: Review of summation-by-parts schemes for initial-boundary-value problems. J. Comput. Phys. **268**, 17–38 (2014)
47. Tsynkov, S.V.: Numerical solution of problems on unbounded domains. A review. Appl. Numer. Math. **27**, 465–532 (1998)
48. Zisowsky, A.: Discrete transparent boundary conditions for systems of evolution equations. PhD thesis, Technische Universität Berlin, Berlin, Germany (July 2003)
49. Zisowsky, A., Arnold, A., Ehrhardt, M., Koprucki, T.: Discrete transparent boundary conditions for transient kp-schrödinger equations with application to quantum–heterostructures. Numer. Math. Theor. Meth. Appl. **3**(3), 295–337 (2010)